J. Fluid Mech. (1989), *vol.* 208, *pp.* 417–458
Printed in Great Britain

Near-wall structure of a turbulent boundary layer with riblets

By KWING-SO CHOI
British Maritime Technology, 1 Waldegrave Road, Teddington, Middlesex TW11 8LZ, UK

(Received 1 December 1987 and in revised form 2 May 1989)

A detailed wind tunnel study has been carried out on the near-wall turbulence structure over smooth and riblet wall surfaces under zero pressure gradient. Time-average quantities as well as conditionally sampled profiles were obtained using hot-wire/film anemometry, along with a simultaneous flow visualization using the smoke-wire technique and a sheet of laser light. The experimental results indicated a significant change of the structure in the turbulent boundary layer near the riblet surface. The change was confined within a small volume of the flow close to the wall surface. A conceptual model for the sequence of the bursts was then proposed based on an extensive study of the flow visualization, and was supported by the results of conditionally sampled velocity fields. A possible mechanism of turbulent drag reduction by riblets is discussed.

1. Introduction

As a result of the 'discovery' of coherent structures in turbulent shear flows (Kline *et al.* 1967; Brown & Roshko 1974) a large number of studies concerning the manipulation or management of turbulent flow have started in the last decade. The concept of using a riblet surface, i.e. a surface with longitudinal micro-grooves, to obtain a skin-friction drag reduction by modifying the coherent structures of the turbulent boundary layer has its origin in these studies and is now very close to industrial application.

The investigation of a passive drag-reduction device with surface modification was initiated by Walsh (Walsh & Weinstein 1978; Walsh 1980, 1982; Walsh & Lindeman 1984) at NASA Langley Research Center, who studied several different types of riblet surfaces parametrically and found that the size of riblets should basically be of the order of the viscous-sublayer thickness in order to gain a net drag reduction. Walsh obtained a net reduction of up to 8% from a surface with triangular ribs. A similar experiment was carried out by Sawyer at the Royal Aerospace Establishment, Bedford, UK (Sawyer & Winter 1986) and NASA's basic results were confirmed. Choi, Pearcey & Savill (1987) conducted towing tank and wind tunnel tests of riblets on a streamlined three-dimensional body and successfully demonstrated the effectiveness of the passive drag-reduction device over a double-curvature surface with non-zero pressure gradient. Compressibility and Reynolds-number effects on riblets were investigated in flight (McLean, George-Falvy & Sullivan 1987) and in a high-speed tunnel (Squire & Savill 1987). They both found net drag reductions even at these conditions. Efforts were also made by several other researchers (Johansen & Smith 1983; Hooshmand, Young & Wallace 1983; Gallagher & Thomas 1984; Bacher & Smith 1985; Bechert, Hoppe & Reif 1985; Bechert *et al.* 1986; Choi 1985, 1986*b*, 1987*a*, *b*; Dinkelacker, Nitschke-Kowsky & Reif 1987; Coustols & Cousteix 1986,

1988; Nieuwstadt *et al.* 1986; Pulles 1988; Reidy 1987; Reidy & Anderson 1988; Djenidi *et al.* 1988) who investigated the difference in turbulence structure of the boundary layer between a riblet surface and a smooth surface. There are, however, anomalies in some of the turbulence statistics measured over the riblet surface, indicating that the structure of the boundary layer modified with riblets is not yet fully understood. For example, the burst frequency was found to be increased by Hooshmand *et al.* (1983) and Pulles (1988), unchanged by Walsh (1982) and Bacher & Smith (1985), and reduced by Gallagher & Thomas (1984) and Savill (1987). For an extensive review of recent developments in riblets as a passive drag-reducing device, readers are referred to the papers by Choi (1984), Johansson & Alfredsson (1985), Bandyopadhyay (1986) and Wilkinson *et al.* (1987). An article by Savill, Truong & Ryhming (1988) includes a summary of recent studies conducted in Europe and different shapes of riblets investigated.

For a possible mechanism of turbulent drag reduction with riblets, several concepts have been proposed. Bacher & Smith (1985) considered the interaction of the counter-rotating longitudinal vortices with the small eddies created by them near the peaks of riblets, arguing that the secondary vortices would act to weaken the longitudinal vortices as well as to retain the low-speed fluid within the grooves. Choi (1984) discussed the mechanism in terms of the increase of spanwise effective viscosity and the thickening of the viscous sublayer which is analogous to the case of drag-reducing polymers. Later Choi (1985, 1986*a*) proposed a new look at the near-wall structure of the turbulent boundary layer based on an extensive study of flow visualization, in which he suggested that the restriction of spanwise movement of longitudinal vortices by the riblets would have a prime responsibility for the turbulent drag reduction. The conceptual model accounting for this mechanism is similar to the one proposed by Wallace (1982), based on the vortex dynamics of bounded shear flows. Head & Bandyopadhyay (1981) have presented strong evidence of these models with flow visualization pictures of counter-rotating pairs of vortices in a smoke-filled turbulent boundary layer. Bechert *et al.* (1985, 1986) also suggested a similar mechanism where they argued that the riblet ridges would impede the cross-flow efficiency of the momentum exchange, thereby leading to a reduction of turbulent skin friction. They then analysed the computational results of viscous Couette flow over riblets in terms of a quantity called the protrusion height, a measure of the influence of the riblets upon the boundary layer. From the results they were able to correlate the amount of turbulent drag reduction with the protrusion height for several different types of riblets, concluding that the height by which the riblets protrude into the boundary-layer flow is of crucial importance.

It should be emphasized that the purpose of investigating the structure of a turbulent boundary layer manipulated with drag-reducing riblets is not limited to the technical development of the devices. Also, it is to promote a better understanding of fluid mechanics, and turbulent shear flows in particular.

In the present paper, a detailed study of near-wall turbulent structure over a riblet surface is described and the results compared with their counterparts over a smooth surface. Time-averaged quantities as well as conditionally sampled flow fields are investigated, revealing the differences in the structure of the turbulent boundary layers. Also presented are the results of simultaneous flow visualization with hot-film anemometry. A conceptual model for the sequence of the bursts is proposed. This is strongly supported by the results of the conditionally sampled velocity fields. Finally, the conceptual model is used along with the experimental data to explain a possible mechanism of turbulent drag reduction with riblets.

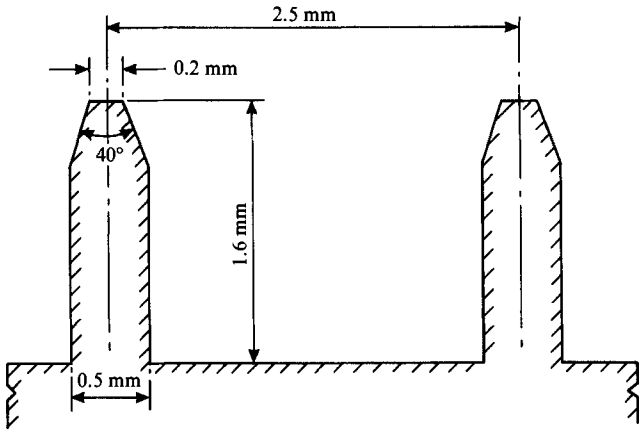

FIGURE 1. Cross-section of riblets.

2. Experimental set-up and procedure

All the experimental studies were carried out at British Maritime Technology in Teddington, UK, using its environmental wind tunnel. The tunnel has a test section 4.8 m wide, 2.4 m high and 15 m long and the flow speed was controllable to within 0.5% of the reading. Hot-wire/film anemometry was used for the mean and turbulence measurements using a constant-temperature system (DISA 55M). We have used DISA miniature hot-wire probes and TSI surface-flushed mounted hot-film sensors with an overheat ratio of 1.8 and 1.2, respectively. The buoyancy effects for these measurements are considered to be negligible at the present test conditions (Collis & Williams 1959). Two interchangeable plates 400 mm wide and 600 mm long were machine cut from soft steel and available for the experiment, one with a smooth surface and the other with a riblet surface. The cross-section of the riblets is given in figure 1. These were placed on the tunnel floor 11 m from the beginning of the test section. The size of the turbulent eddies, which are affected by the change in the boundary condition imposed by the riblets, is of the order of the size of the riblets, so that the timescale of these eddies is also small. The length of the test plate (600 mm), which is nearly twice the boundary-layer thickness, is, therefore, long enough for the purpose of the present study of the near-wall turbulent structure. In fact, our recent experimental results suggested that the near-wall structure of the turbulent boundary layer responds to a change of the surface condition from smooth to riblet within 400 wall units, equivalent to 50 mm for the present experiment (Choi & Johnson 1989).

The height and width of the riblets were 13 and 20 wall units respectively, with a mean free-stream velocity of 3 m/s. For the flow visualization study, the velocity was reduced to 1.5 m/s in order to record pictures of better resolution. This lower speed did not impair the effectiveness of the riblets.

At the location of test plates a uniform mean velocity profile of the naturally grown turbulent boundary layer was observed for a span of approximately 1000 mm. The momentum thickness was 21.6 ± 1.0 mm and the thickness of the viscous sublayer was about 1.3 mm. The Reynolds numbers based on the momentum thickness and the shape factor of the boundary layer were 4.6×10^3 and 1.34.

3. Mean velocity and turbulence intensity profiles

Similar to the flow over the rough surfaces, the turbulent boundary layer over the riblets does not have predefined origin for height. Several efforts have been made in the past, both experimentally and analytically, to determine the virtual origin of mean velocity profiles over a riblet surface. Hooshmand *et al.* (1983) used a subminiature hot-wire to measure mean velocity and turbulence intensity profiles over the peaks and valleys of a riblet surface. He concluded that the virtual origin was zero over the peaks and one half the riblet height over the valleys. Bechert *et al.* (1985, 1986) analysed the computed velocity profiles for viscous Couette flow, and obtained the 'protrusion height' of the riblets by matching the velocity profile with that over a smooth surface. According to the results, the protrusion height divided by the riblet height (h) was found to be 0.25 for triangular riblets and 0.37 for scalloped riblets for h/S equal to 0.6 (the value corresponding to the present experiment, where S is the riblet spacing). Squire & Savill (1987) successfully made use of an assumed virtual origin of a quarter riblet height from the peak in plotting their velocity profiles for transonic speeds.

In the present study, we employed a method of Furuya & Fujita (1966) for their investigation of the turbulent boundary layer over a rough surface. They defined the virtual origin in such a way that the mean velocity profiles can be expressed by the log-law in the overlapped region of the inner and outer region. With this definition, they plotted $(U_\infty - u)/u^*$ *vs.* $yu^*/\delta U_\infty$ for different values of virtual origin y_v, and took the value that gave the best fit to the velocity defect profile for a rough surface.

This method can be applied to the present case provided we know the skin-friction velocity u^*. However, since u^* was not measured the method has been modified so that we could obtain y_v and u^* at the same time. In our method, an assumption was made that the non-dimensional defect velocity profile $(U_\infty - u)/u^*$ on a riblet surface should take the same shape as that on a smooth surface when it is plotted against the non-dimensional distance $yu^*/\delta^* U_\infty$, except for the inner region of the turbulent boundary layer. A similar technique has been suggested by Bandyopadhyay (1986) and it was tested by Squire & Savill (1987) with a good result for the triangular riblets of $h^+ = 20$.

To apply the method, the defect velocity profile $(U_\infty - u)/u^*$ *vs.* $yu^*/\delta^* U_\infty$ over the smooth surface was expressed in terms of a fourth-order polynomial for the overlapped region ($0.002 < yu^*/\delta^* U_\infty < 0.15$) of the turbulent boundary layer. Then, the defect velocity profile of the turbulent boundary layer over the riblet surface was plotted in the same manner and the best fit to the polynomial was sought by changing the value of two parameters y_v and u^*, each time re-evaluating δ^*. The best fit was achieved after a few iterations with $u^* = 0.1136$ m/s and $y_v = 0.22$ mm. By comparing these values with those over the smooth surface, the skin-friction velocity was found to be 1.5% smaller, equivalent to 3% reduction in skin-friction drag. The virtual origin measured downwards from the top of the riblets was 0.15 times the riblet height. This is slightly smaller than the findings of Hooshmand *et al.* (1983) and Bechert *et al.* (1985, 1986).

The skin-friction velocity of the turbulent boundary layer over a smooth surface was obtained using a Clauser plot. The log-law profile to which we fitted the experimental data was

$$\frac{u}{u^*} = 5.5 \log \frac{yu^*}{\nu} + 5.45, \tag{1}$$

	Mean value	Variations
u^* m/s	0.115	± 0.003
θ mm	21.8	± 1.0
H	1.34	± 0.01

TABLE 1. Skin-friction velocity u^* and integral parameters θ and H over the smooth surface

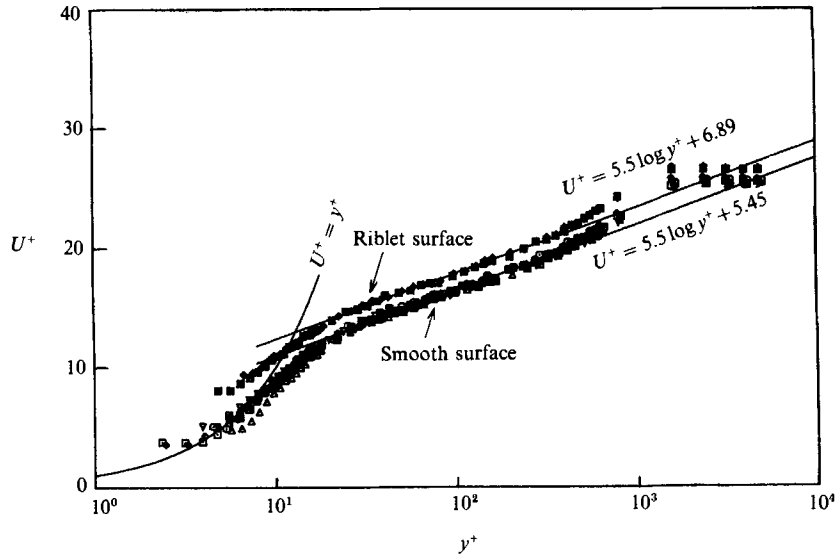

FIGURE 2. The log–law plot of mean velocity profiles over smooth and riblet surfaces.

suggested by Patel (1965). Six velocity profiles, taken at different spanwise positions (-150 mm $< y <$ 150 mm), were used in this process. The values of u^* are given in table 1 along with the corresponding values of the momentum thickness and shape factor.

A log-law plot of the mean velocity profiles is given in figure 2 for both the smooth surface and riblet surface. Included in the figure are the six sets of data at different spanwise positions. The extent to which the mean velocity followed the logarithmic law was quite wide, certainly more than a decade ($30 < y^+ < 400$), reflecting the reasonably large Reynolds number (4.6×10^3 based on the momentum thickness) of this experiment. The slope of the log law over the riblet surface remained the same as that of the smooth surface; however, the intercept of the law was increased from the value 5.45 of the smooth surface to 6.89. The log law for the riblet surface is therefore given by

$$u^+ = 5.5 \log y^+ + 6.89. \tag{2}$$

This upward shift in the velocity profile has been observed in other riblets studies (Hooshmand *et al.* 1983) as well as with large-eddy breakup (LEBU) devices (see Bandyopadhyay 1986 and Nguyen, Savill & Westphal 1987). It is also a common phenomenon of drag reduction using long-chain polymers (Lumley 1973; Virk 1975). The upward shift can be considered as an adjustment of the balance between the turbulence energy production and the viscous dissipation, which is reflected by a

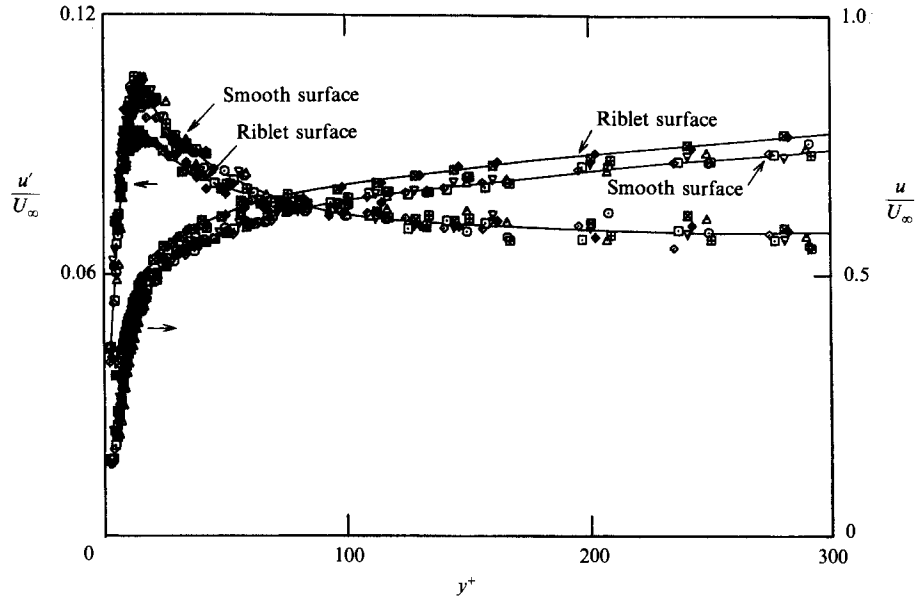

FIGURE 3. The turbulence intensity and mean velocity profiles for the turbulent boundary layer over smooth and riblet surfaces.

change of viscous-sublayer thickness or the smallest size of turbulent eddies in the boundary layer (Lumley 1973). Therefore the turbulence energy production is less with an upward shift of the log-law curve, resulting in the reduction of turbulent drag (Choi 1984).

Mean velocity and turbulence intensity profiles in the inner region of the turbulent boundary layer over a smooth and a riblet surface are plotted in figure 3 against y^+ using a linear scale. Again, all the spanwise sets of data are plotted. As shown in figure 3 an increase of u/U_∞ over the riblet surface is noticeable compared to that over the smooth surface. This increase can be seen in the log plot given in figure 2 as an increase of intercept. Turbulence intensity u'/U_∞ was reduced by up to 10% over the riblet surface compared with the smooth surface. However, this reduction was observed only in the near-wall region, say $y^+ < 70$. The maximum turbulence intensity was at $y^+ = 18$ with $u'/U_\infty = 0.104$ over the smooth surface, while it was at $y^+ = 19$ over the riblet surface with $u'/U_\infty = 0.0934$. These data compare reasonably well with others. For example, the experiment by Klebanoff (1955) for a smooth surface indicated the maximum value of $u'/U_\infty = 0.113$ at $y^+ = 23$, and Hooshmand *et al.* (1983) obtained the maximum $u'/U_\infty = 0.114$ at $y^+ = 20$. Hooshmand *et al.* also gave data on a triangular riblet surface, which showed that the maximum turbulence intensity $u'/U_\infty = 0.100$ was observed at $y^+ = 16$.

The reduction of turbulence intensity over the riblet surface observed here suggests that the level of wall-pressure fluctuation p'_w might also be reduced over the riblet surface. This is indeed the case and the results of the wall-pressure measurement by Choi (1987*a*) showed a reduction of p'_w by 4%.

4. Skin-friction measurements

Measurements of skin friction using surface hot-film sensors were carried out extensively in the course of the present investigation, since they represent the

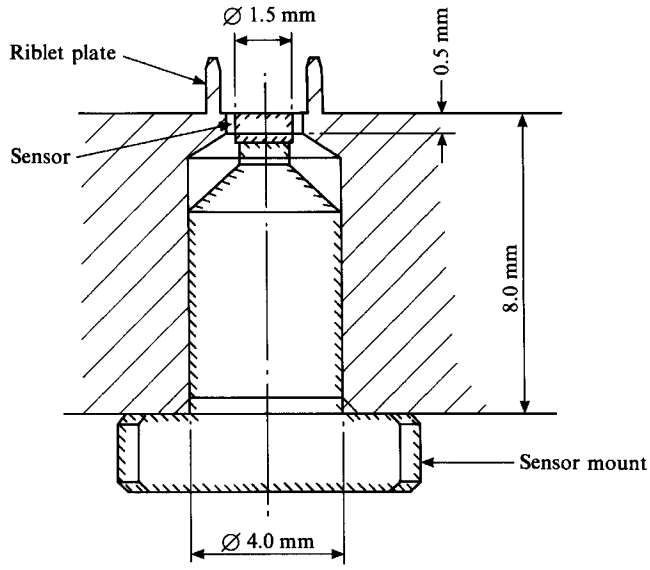

FIGURE 4. The hot-film sensor and the mount for the riblet test.

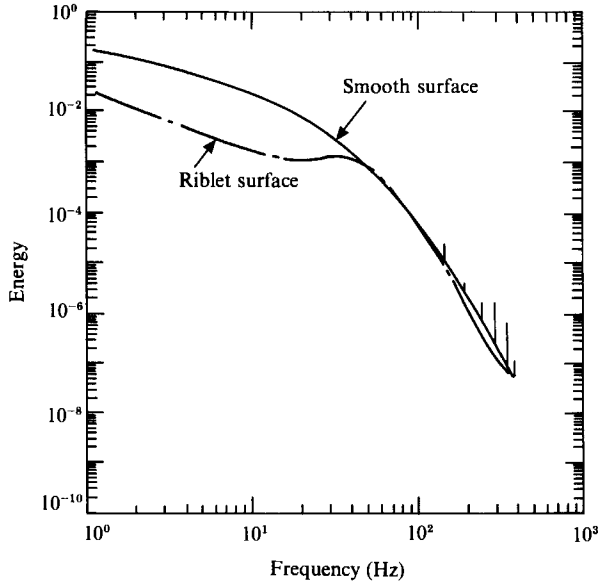

FIGURE 5. Spectra of wall-skin-friction fluctuation for the smooth and riblet surfaces.

immediate consequences of the change in boundary conditions imposed by riblets. Initial emphasis was placed on the investigation of differences in their signatures and the spectral contents. The sensors (TSI 1471), whose platinum heating elements were covered with cylindrical quartz of 1.5 mm diameter and 0.7 mm height, were mounted flush with either the smooth surface or the bottom surface of the riblets (figure 4). The low-frequency response of these sensors was believed to be impaired owing to the heat loss to the substrate. The hot-film data were, therefore, used only for comparative purposes between the two surfaces.

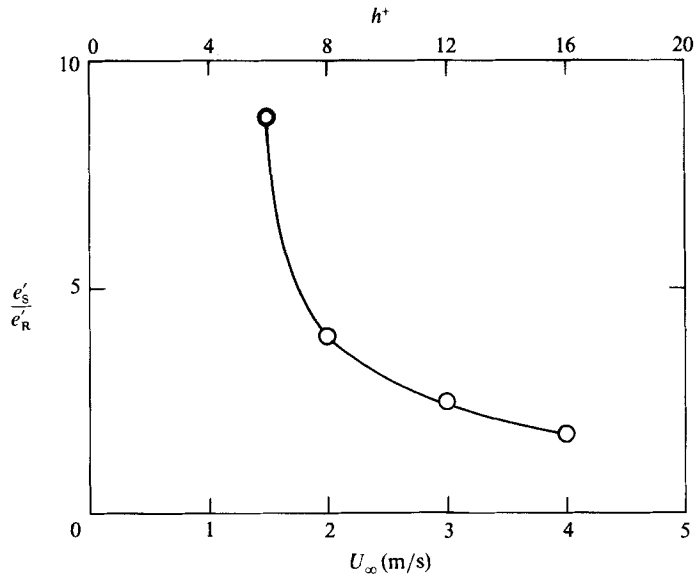

FIGURE 6. Ratio of r.m.s. intensities of skin-friction fluctuation between the smooth surface e'_S and riblet surface e'_R as a function of the free-stream velocity U_∞ and non-dimensional riblet height h^+.

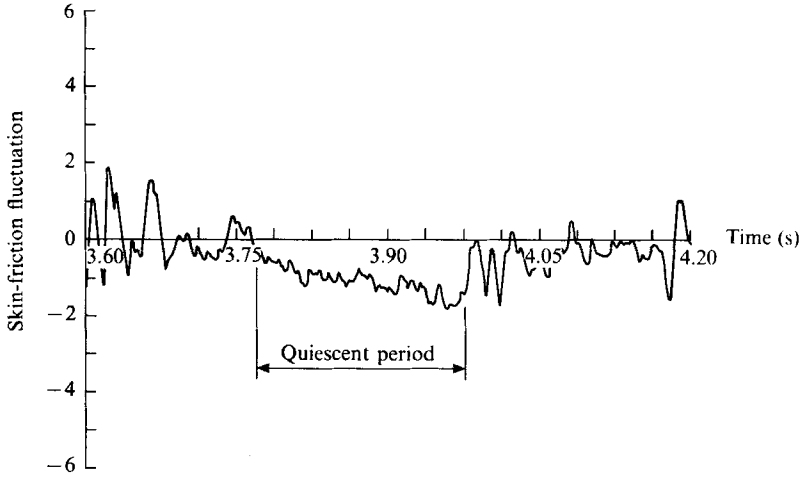

FIGURE 7. A period of quiescence in the turbulence activities observed in a recorded signal of wall-skin friction fluctuation.

Skin-friction spectra for a free-stream velocity of 3 m/s are plotted in figure 5. From this figure it is clear that the reduction of energy in surface skin friction by riblets was confined to the lower-frequency part of the spectrum (say, less than 50 Hz). There was, however, a frequency range between 50 Hz and 100 Hz where the energy content in the spectrum for the riblet surface was larger than that for the smooth surface. It is believed that the increase in the energy content in this range was due to the increase in burst frequency over the riblet surface (Choi 1985). Although riblets are small-scale features, they can affect the sequence of large-scale burst events by restricting the lateral movement of the vortex structure (Choi

1987*a*). This results in the reduction of the skin-friction spectrum at lower frequencies.

Figure 6 shows the results of the r.m.s. intensity of skin-friction fluctuations for free-stream velocities of 2, 3 and 4 m/s. (Data point at $U_\infty = 1.5$ m/s is from Choi 1985.) The quantity e'_S/e'_R is plotted against h^+ as well as U_∞. The figure shows that the ratio e'_S/e'_R increased from 1.78 at $h^+ = 16$ ($U_\infty = 4$ m/s) to 8.76 at $h^+ = 6$ ($U_\infty = 1.5$ m/s), indicating a significant reduction in the r.m.s. intensity by riblets. They were still within the effective riblet height for drag reduction.

Sandborn (1981) measured both r.m.s. and mean values of wall skin friction of a turbulent boundary layer downstream of riblet-like fences. The result indicated that there is a strong correlation between the reductions in r.m.s. intensities and mean values of wall skin friction. Our results are, therefore, interpreted to indicate that there is a large skin-friction reduction over the riblet surface, at least locally between the ribs. This may explain why riblets produce a net drag reduction in spite of the increase in surface area (Bandyopadhyay 1986).

As the reduction in r.m.s. intensity of the skin-friction signal at the riblet surface was so large, the fluctuating component of the skin-friction signal was carefully studied. The inspection revealed that there were short periods of quiescence in the turbulence activity in the signal. A typical example is shown in figure 7, in which an approximately 0.2 s ($t^+ = tu^{*2}/\nu \approx 170$) quiescent period was observed in the signal obtained with the free-stream velocity of 3 m/s, corresponding to the non-dimensional riblet height of $h^+ = 12$. This period of quiescent turbulence seems to be due to the partial laminarization of the viscous sublayer near the bottom of the riblets. Similar findings were made by many other investigators (Hooshmand *et al.* 1983; Gallagher & Thomas 1984; Bacher & Smith 1985). Notably, Gallagher & Thomas observed during their flow visualization study that the dye formed a quiescent and viscous-like pool between the ribs, and it left the groove only when a burst passed overhead.

5. Wall-pressure measurements

The measurements of wall-pressure fluctuations were carried out using a half-inch probe microphone (Bruel & Kjaer Type 4166), fitted to the sensor hole used for the skin-friction measurements. The end surface of the probe with 1.6 mm inner diameter ($d^+ = du^*/\nu = 13$) was flush with the surrounding surface of the test plate. The total length of the probe was 23 mm and the cavity volume in front of the diaphragm was less than 20 mm^3. The calibration of the probe microphone was carried out using a 2 cm^3 coupler. The frequency response of the probe microphone was flat (within 1.0 dB) from 10 Hz up to 400 Hz, the Nyquist frequency for the sampling.

As it was found that the signal-to-noise ratio of wall-pressure fluctuation was low (about 10 dB) owing to the acoustic noise of the tunnel, many short-time data were acquired when the free-stream velocity in the wind tunnel dropped to 3 m/s after shutting off the power switch. This resulted in an improvement of the signal-to-noise ratio by nearly 15 dB. Typically about three hundred data sets, each consisting of 2050 data points at the sampling rate of 800 Hz, were used to obtain a spectrum of the wall-pressure fluctuations. The flow was not completely steady during the data acquisition; however, the deceleration of the flow in the tunnel was very small (0.078 m/s^2). Therefore, the 'memory effect' should be small enough to enable us to compare the spectra between two different surfaces.

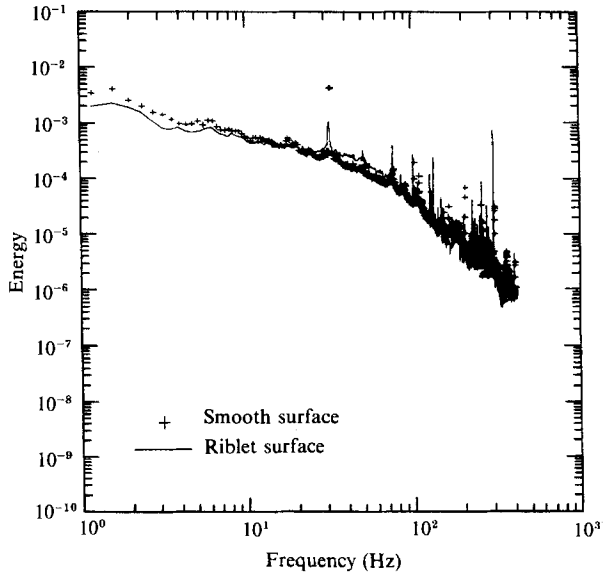

FIGURE 8. Spectra of wall-pressure fluctuations on smooth and riblet surfaces.

The results of wall-pressure spectra for the smooth surface (indicated with +) and the riblet surface (indicated with a solid line) are given in figure 8. The energy in the wall-pressure fluctuations was less on the riblet surface at the lower frequencies, below say 20 Hz, whilst there was an increase at the higher frequencies, between 20 Hz to 100 Hz. No change was evident above 100 Hz. The wall-pressure spectra were numerically integrated to give the r.m.s. intensity p'_w. The intensity p'_w on the riblet surface was about 4% smaller than that on the smooth surface.

When these spectra are compared with the spectra of skin-friction fluctuations in figure 5, they both demonstrate similar characteristics. The spectra for the riblet surface show reductions of energy at lower frequencies (i.e. under 50 Hz for skin friction, and below 20 Hz for wall pressure) and slight increases at higher frequencies up to 100 Hz. Above 100 Hz changes in the spectra are not observed.

Overall, the changes in the wall-pressure spectrum at the riblet surface are very similar to those obtained by Beeler (1986) who found that the energy content at lower frequencies was reduced owing to the modification of the boundary layer with an LEBU device. Beeler also demonstrated that p'_w in the LEBU-modified turbulent boundary layer was 12.5% less than that of an unmodified boundary layer. Choi (1987*a*) argued that the different amount of reduction in p'_w between the riblets and the LEBU device was due to different reductions in the turbulence level across the boundary layer. Compared to the present results over the riblet surface where a moderate reduction (about 10%) in the turbulence intensity was observed within the near-wall region, say $y^+ < 70$, LEBU devices produce a larger reduction of around 30% across the entire boundary-layer thickness (Blackwelder & Chang 1986; Guezennec & Nagib 1985).

6. Conceptual model of the burst events

In order to complement the hot-wire/film measurements, a flow visualization of the near-wall turbulence structure was carried out using the smoke-wire streak technique (Choi 1985) with a sheet of laser light. A nickel chrome wire of 0.1 mm (0.4

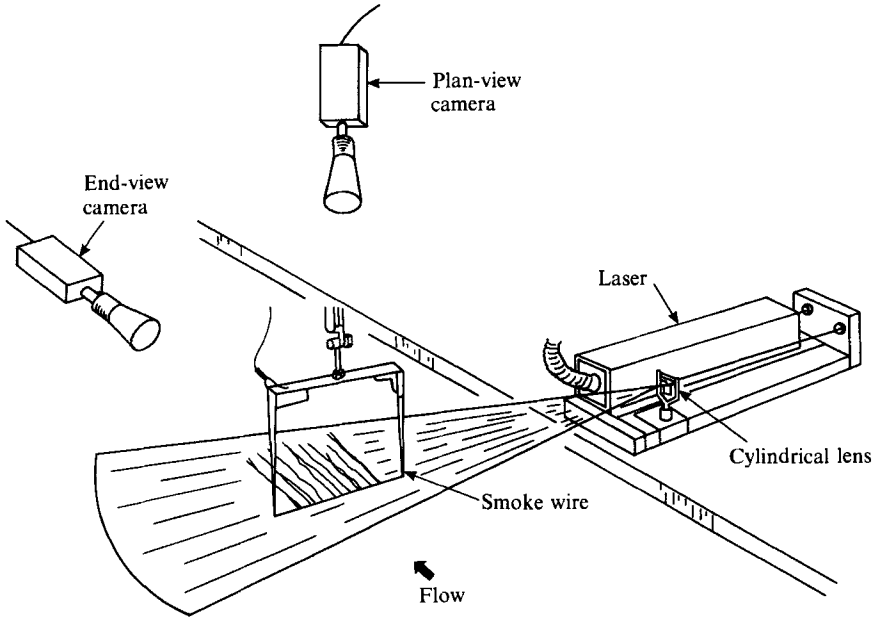

FIGURE 9. Experimental set-up for the flow visualization.

wall units) in diameter, used for the smoke wire, was spray painted to produce marks at a regular interval (3.2 mm, 13 wall units). As the wire was heated by a d.c. current, the temperature of the liquid paraffin, brushed evenly along the wire, increased such that droplets of paraffin were formed with equal spacings. With the formation of these droplets, streaks of white smoke were produced continuously for about one minute. The light sheet, about 1 mm (4 wall units) in thickness over the test plate, was produced by fanning out the beam from the 3 W laser parallel to the wall surface using a cylindrical lens. The laser was positioned such that the light sheet was slightly higher ($y^+ = 8$) than the smoke wire placed at $y^+ = 4$ (see figure 9). Because of this unique positioning of the laser light sheet relative to the smoke wire, we could identify the movement of the flow perpendicular as well as parallel to the wall surface. Whilst the white smoke from the wire was brightly illuminated as it rose into the plane of light, the illumination was less when the smoke sank towards the wall. Two synchronized video cameras (JVC KT-1900E) and U-matic video recorders were used to record the plan view and end view of the flow visualization. The two views were mixed during the recording so that a simultaneous observation of the turbulence structure near the wall surface was possible.

Interpretation and extraction of the essential features from flow visualization pictures are difficult when the flows are unsteady and random. The structure of turbulent flow near a wall surface is a typical example, so that a careful treatment is required in getting information from the pictures. One method to achieve this is to employ anemometry at the same time as the flow visualization. Here we carried out an experiment where a flow visualization was conducted simultaneously with a surface hot-film anemometer to measure the skin-friction fluctuation. For this case, the time-code generator for video pictures was synchronized with the sampling of wall skin friction so that each scene of the flow visualization pictures could be matched exactly with the instantaneous wall-skin-friction signal.

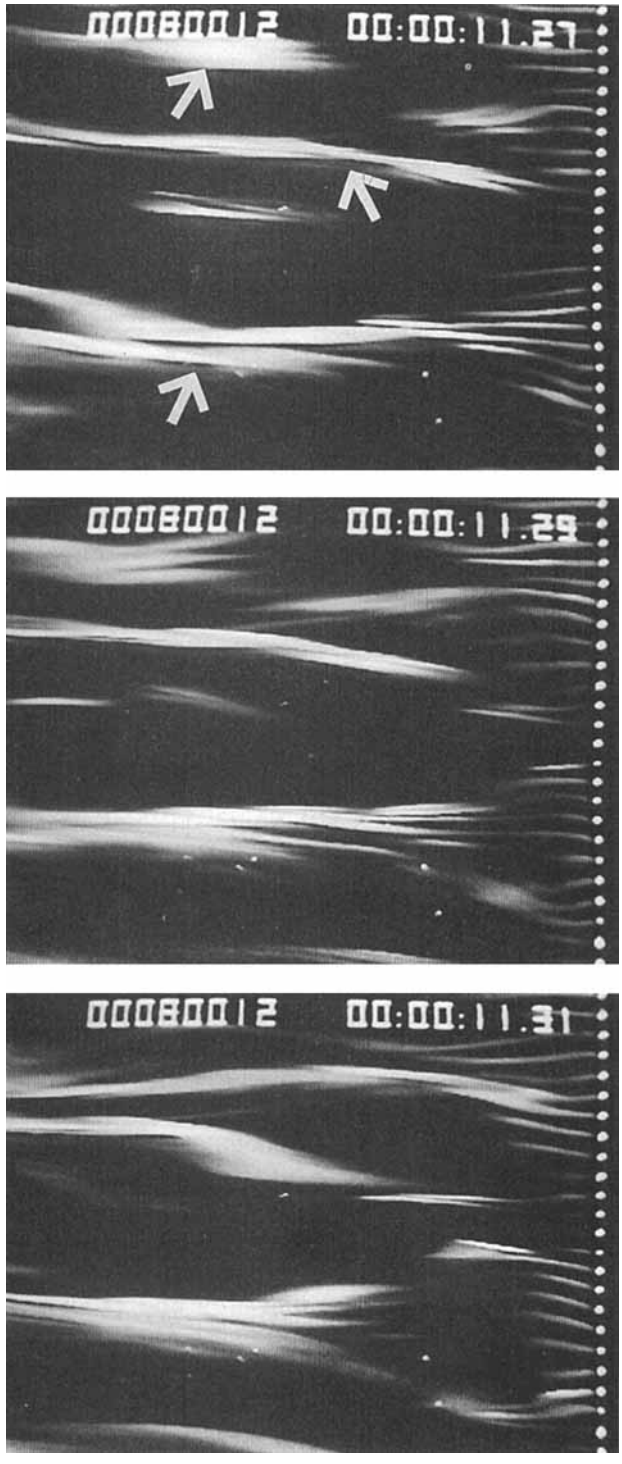

FIGURE 10. For caption see p. 431.

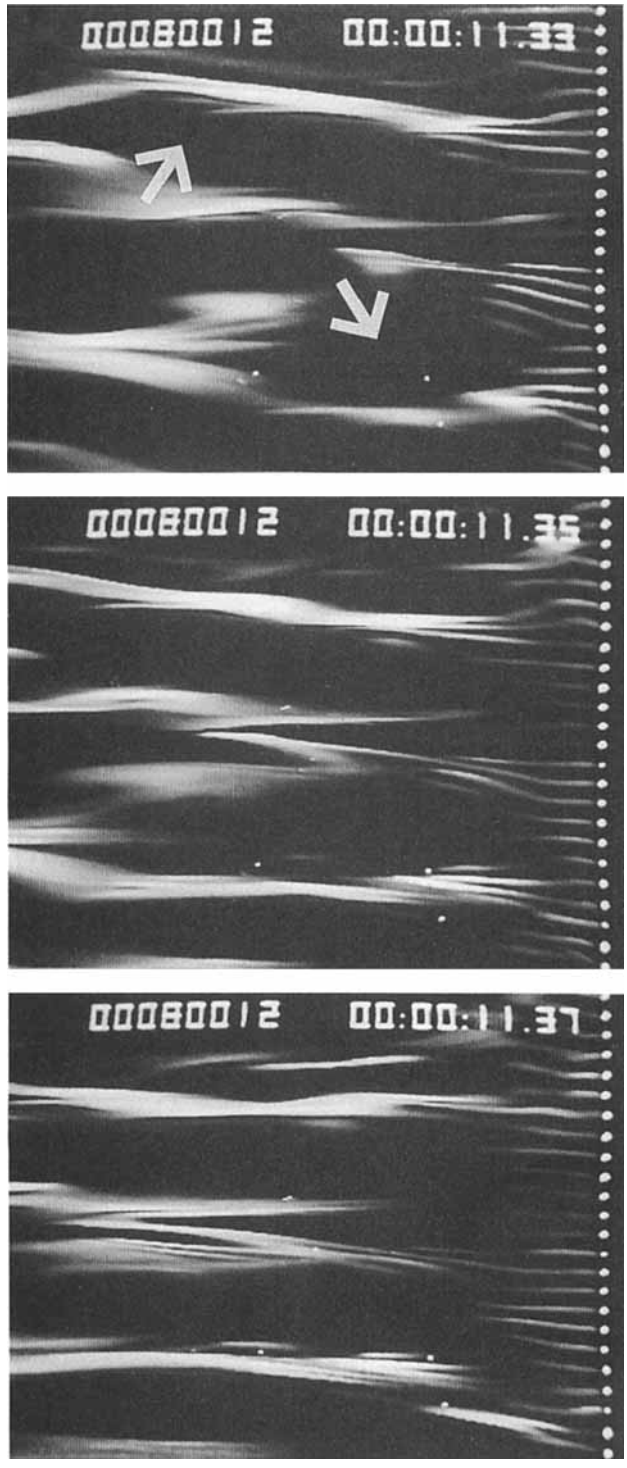

FIGURE 10. For caption see p. 431.

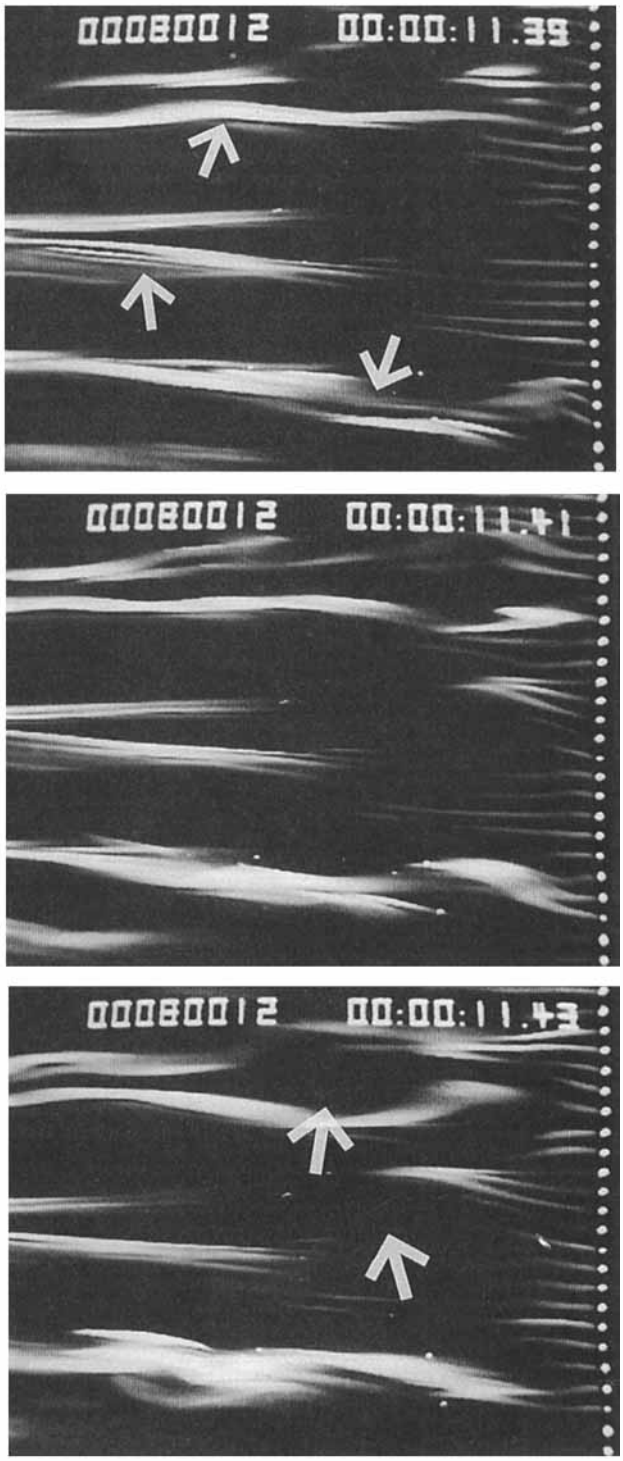

FIGURE 10. For caption see facing page.

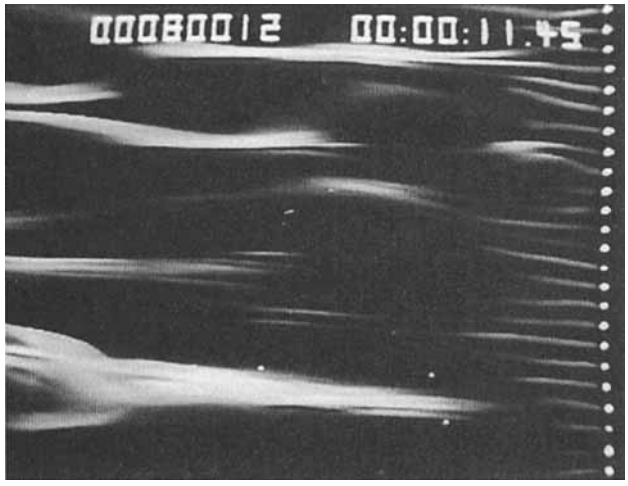

FIGURE 10. A typical sequence of the burst event visualized with the smoke-wire technique with a sheet of laser light. Flow is from right to left.

Figure 10 shows a sequence of burst events over a smooth surface. The free-stream velocity of the boundary layer was set to 1.5 m/s ($R_\theta = 2.7 \times 10^3$). This velocity was found to give the best resolution of flow-visualized pictures. Only the plan view was recorded for this particular sequence of pictures. The flow direction is from right to left, and the smoke wire, with liquid paraffin droplets spaced every 13 wall units, can be seen at the right of each picture. The time code, which indicates the elapsed time in seconds and fiftieths of a second, is shown at the upper right corner. There were twenty-five video frames in every second of recording.

As shown in the pictures, smoke filaments from the smoke wire were tangled up into thick smoke tubes by the vortices in the boundary layer. They were brightly illuminated as they rose from the wall into the plane of laser light. At the beginning of the sequence (time 11:27) there seemed to be two and a half pairs of longitudinal vortices indicated by arrows in the figure which manifested themselves as bright white smoke tubes. The pairs each developed into a loop shape (time 11:29–11:33) creating the next generation of pairs upstream (time 11:39) by joining two neighbouring vortices. The new pair of longitudinal vortices was formed in a staggered fashion upstream of the two parent vortices.

The spanwise spacing between the pairs of longitudinal vortices varied from one scene to another between 90 and 130 wall units (the field of view of the video screen is approximately 300 wall units vertically and 380 wall units horizontally). These values are very similar to those of the low-speed streak spacings (Kline *et al.* 1967), suggesting a possibility that pairs of counter-rotating longitudinal vortices are responsible for the low-speed streaks. It is also believed (Smith & Metzler 1983; Choi 1985, 1986*a*) that these longitudinal pairs of vortices were in fact legs of neighbouring hairpin loops and that they were formed as the hairpin loops were ejected away from the wall during an 'ejection' phase of the burst event. Therefore the loop-shaped smoke tubes observed at time 11:33 and 11:43 of the sequence in figure 10 (shown by arrows) were probably the hairpin loops developed from the lateral vortex filaments imbedded in the boundary layer (Choi 1985).

Figure 11 shows a typical sequence of near-wall turbulence activities recorded on

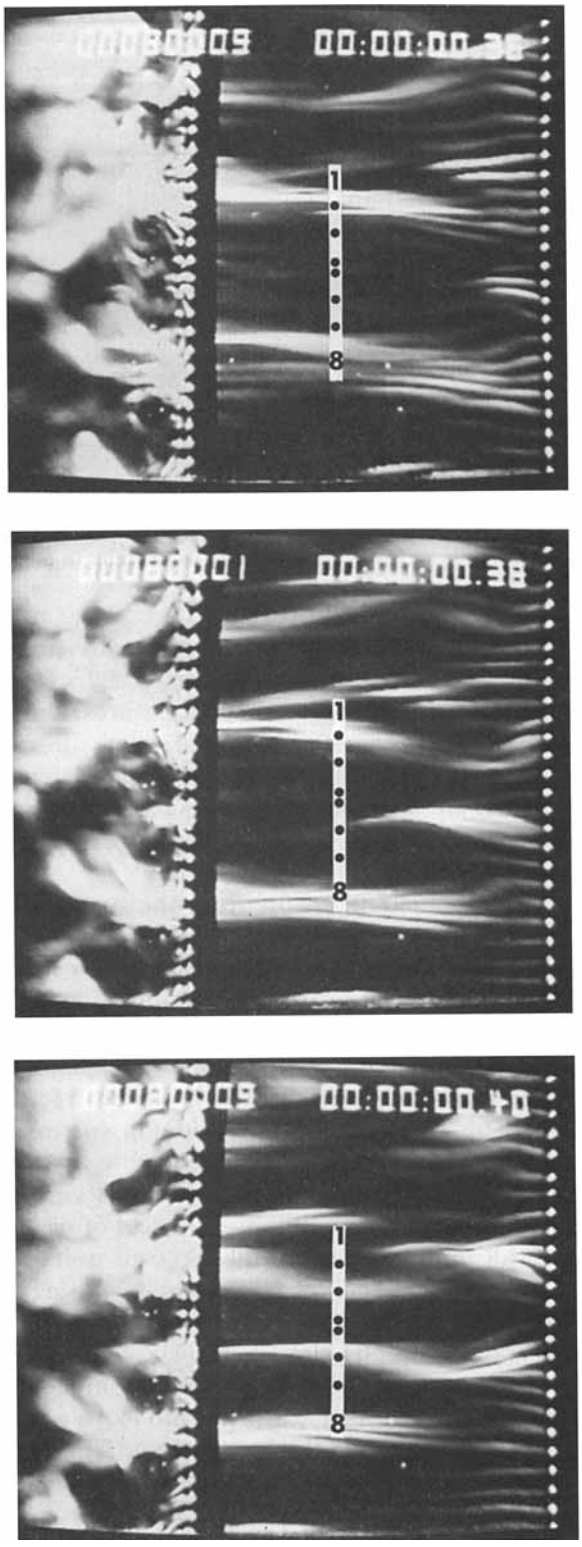

FIGURE 11. For caption see p. 437.

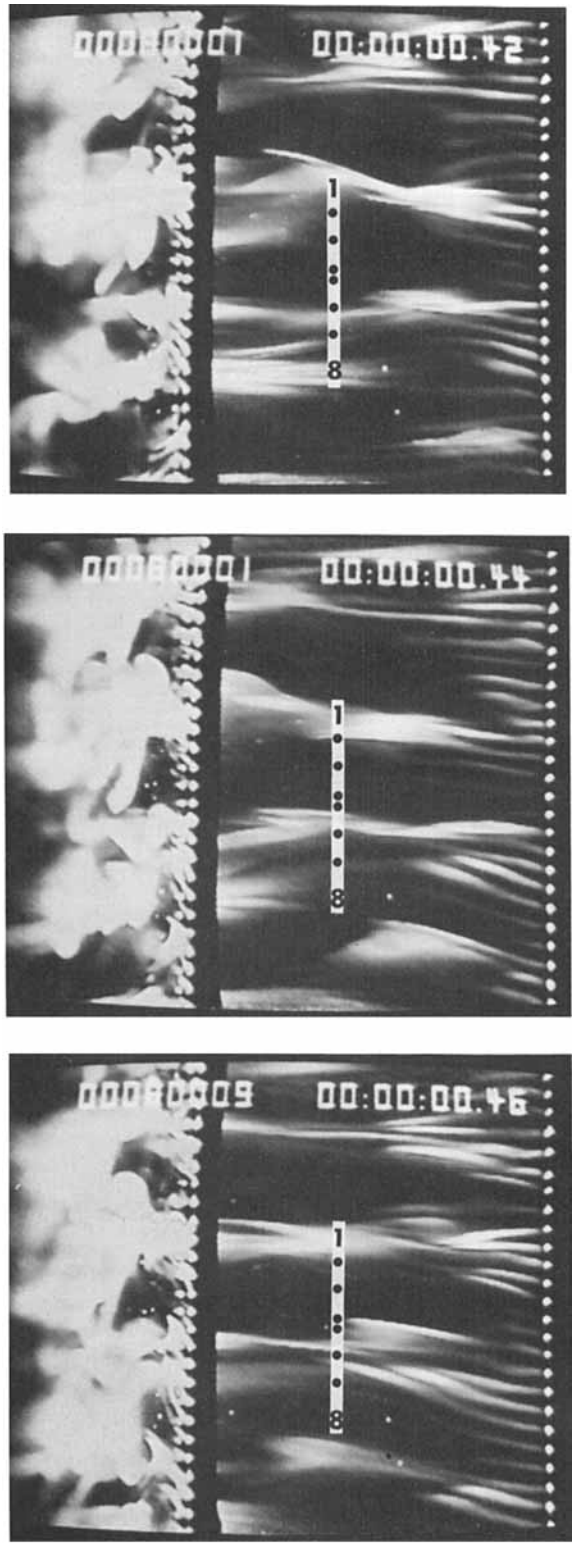

FIGURE 11. For caption see p. 437.

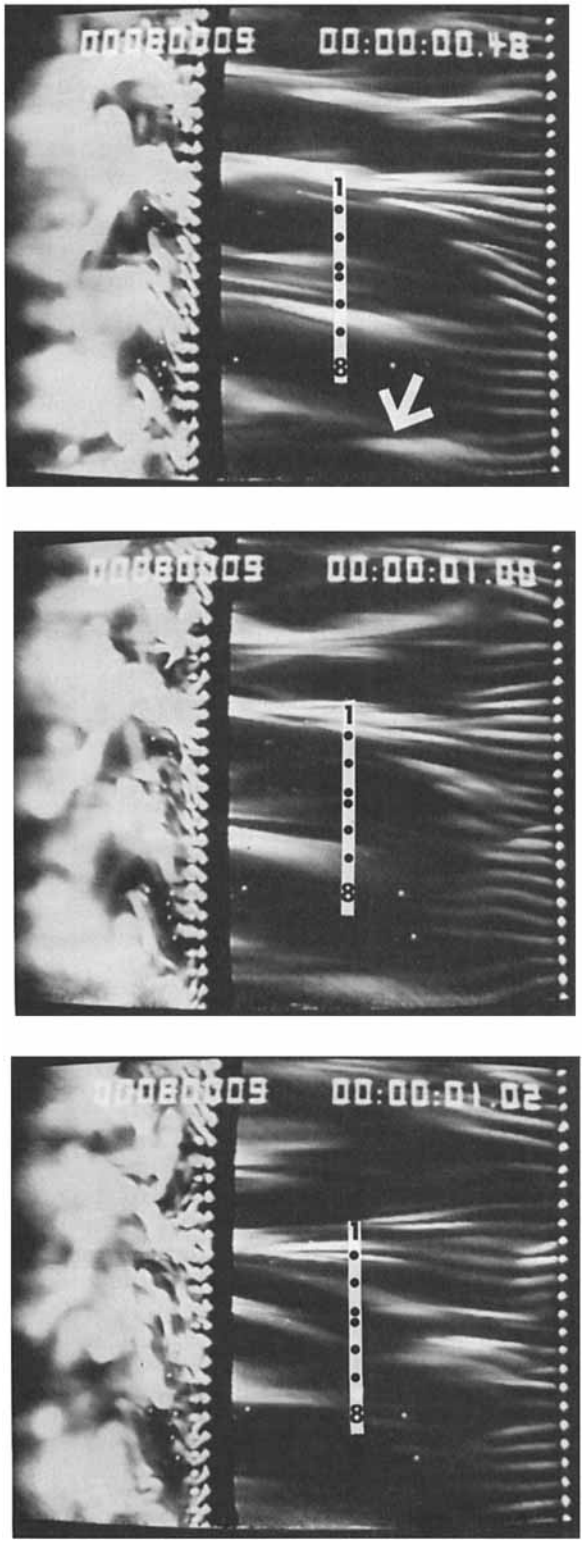

FIGURE 11. For caption see p. 437.

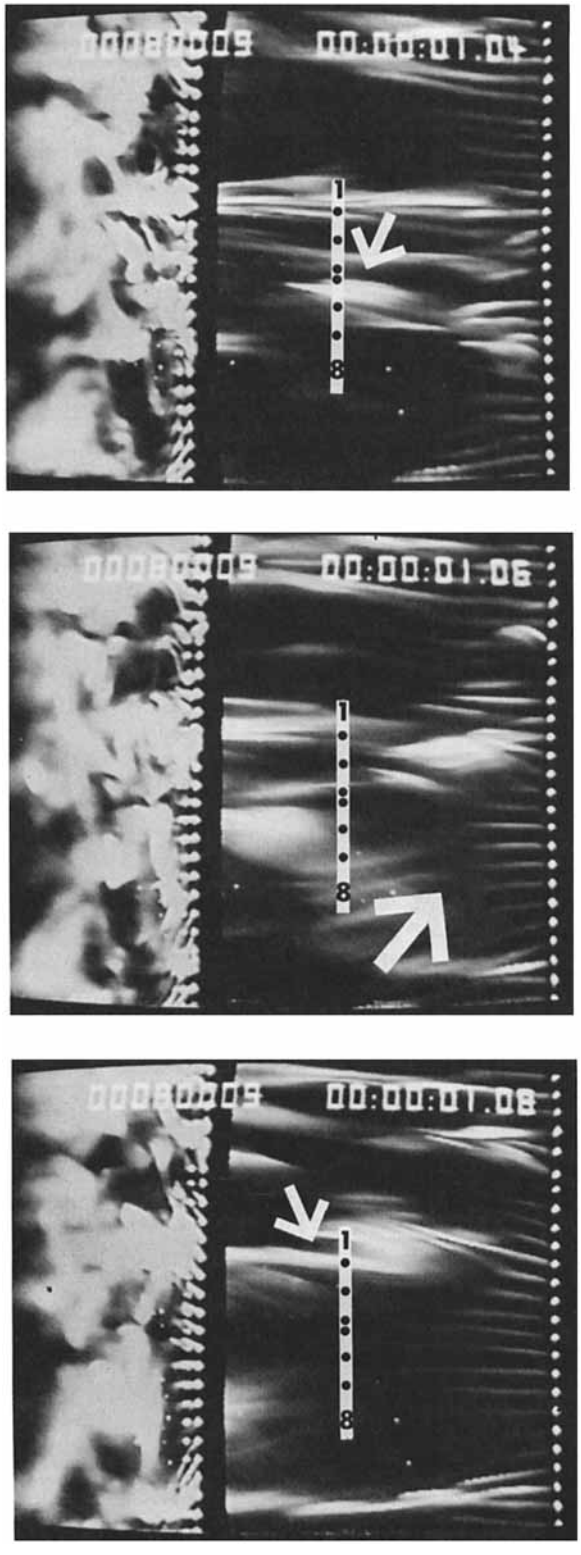

FIGURE 11. For caption see p. 437.

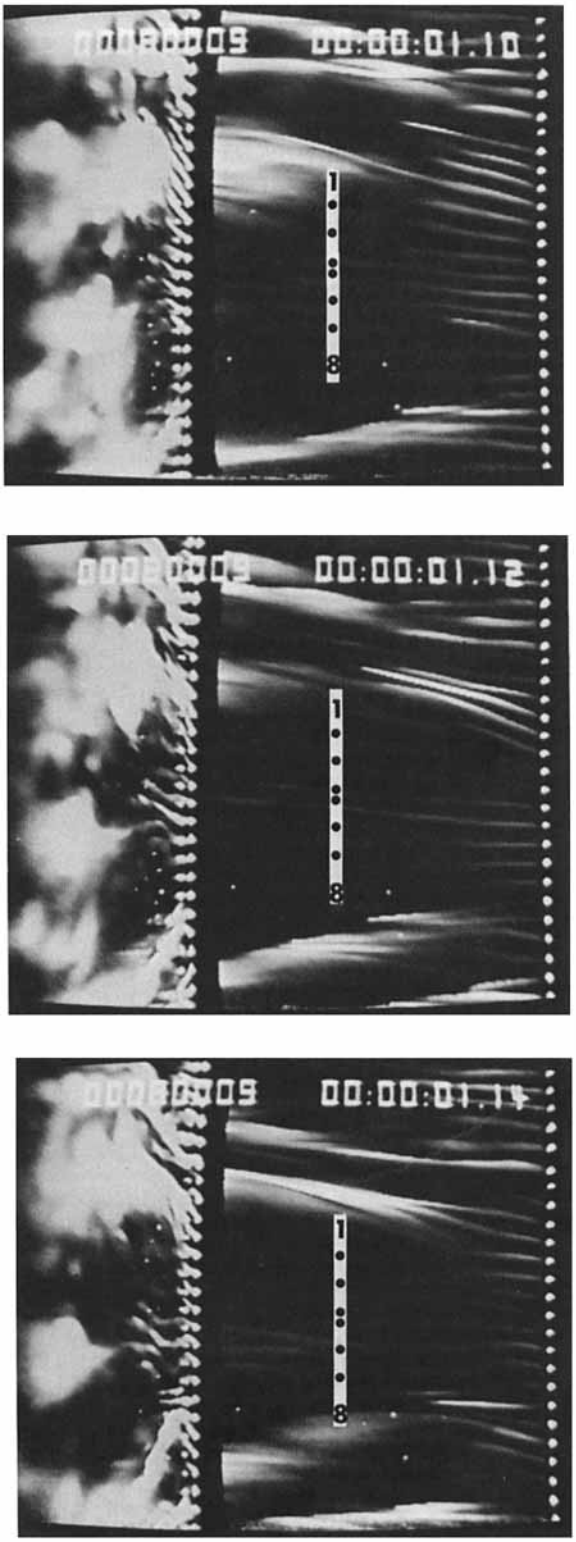

FIGURE 11. For caption see facing page.

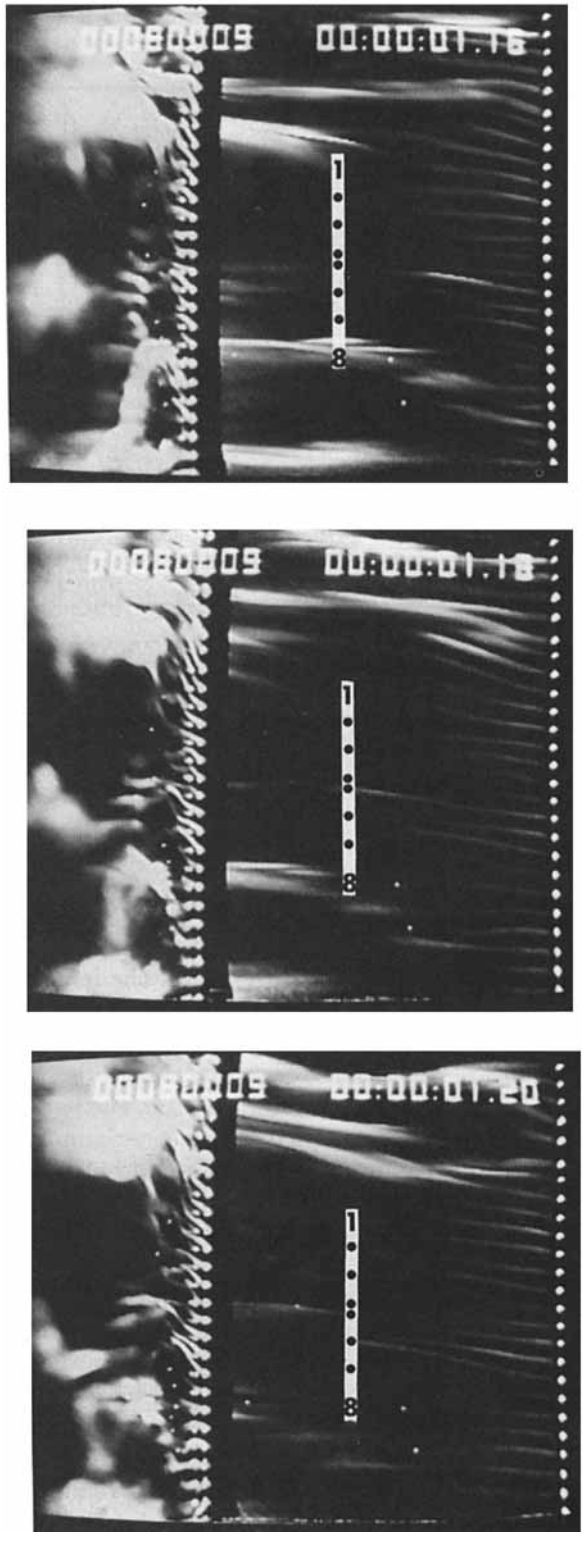

FIGURE 11. A dual-view of near-wall turbulence activities recorded on video tape. Positions of hot-film sensors are indicated by the numbers near the centre of each picture.

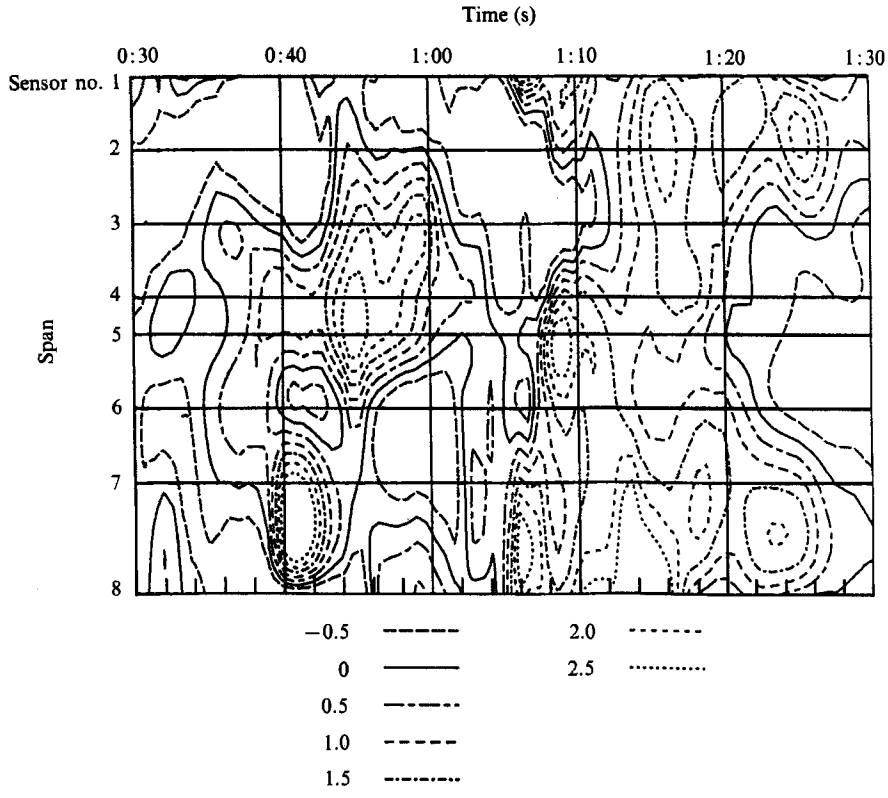

FIGURE 12. Contour map of normalized skin-friction fluctuations. Legend shows the r.m.s. intensity.

video tape. This time the end view, which was recorded simultaneously looking upstream, was superimposed over the plan view on the left of each picture. There were eight hot-film sensors mounted flush with the surrounding surface. The position of each sensors is indicated by its number near the centre of each picture. In figures 12 and 13, contour maps are constructed from the time series of skin-friction signals measured at each sensor position (nos. 1–8 indicated in the figures). They are plotted in such a way that time elapses from left to right corresponding to the direction of mean flow in the flow visualization pictures. Figure 12 shows the fluctuating skin friction normalized with the r.m.s. intensity, and figure 13 indicates the running standard deviation to detect the bursts using the VITA technique. The events associated with a sharp increase of skin-friction fluctuation should be identified with those having dense iso-skin friction contours in figure 12. They should, on the other hand, be found on the peaks of contours in figure 13. The detection of these events, which we call near-wall bursts, is easier with a contour map like figure 13.

Comparing figure 11 with figures 12 and 13, one can see a correlation between pairs of longitudinal vortices, which manifest themselves as bright white smoke tubes, and near-wall bursts. Particular attention should be paid to the end view of the pictures, where rotation of the smoke tubes was noticed. The correlation is particularly clear between the time 0:46 and 1:10 s, where three near-wall bursts were observed sequentially. They took place first at the no. 7 and 8 sensors and then between no. 4 and 6 sensors, and finally at the no. 1 and 2 sensors. These events are indicated

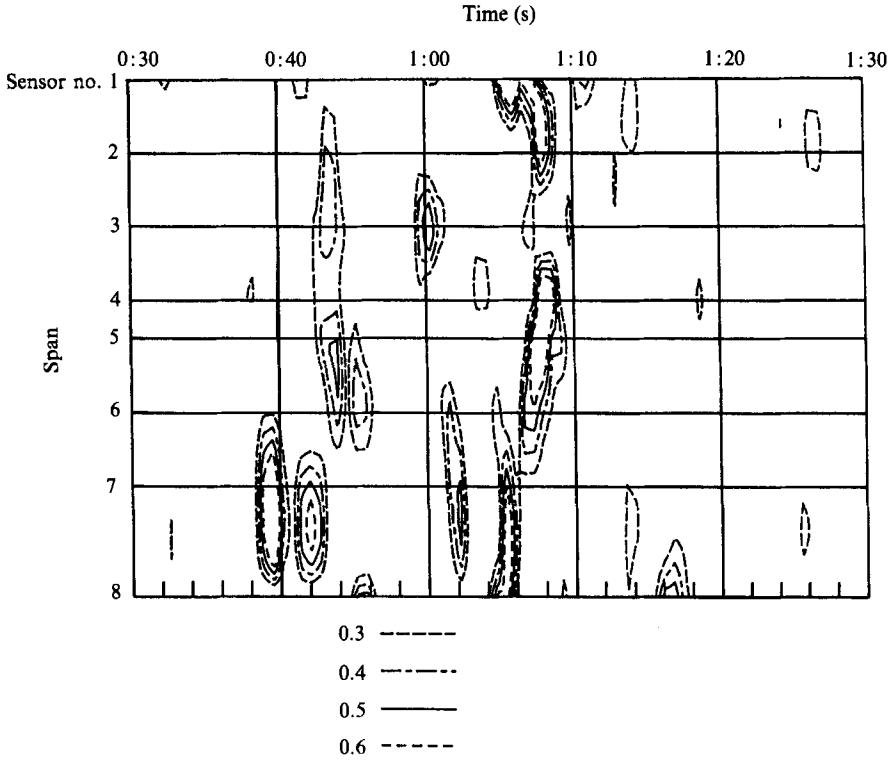

FIGURE 13. Contour map of running standard deviation used for the burst detection using the VITA technique. Legend shows the r.m.s. intensity.

by arrows in figure 11, at times 0:48, 1:04 and 1:08 s, respectively. One can also observe a large-scale fluid displacement away from the wall following the series of near-wall bursts. The displacement of the fluid started immediately after the near-wall burst at the no. 7 and no. 8 sensors at time 1:06 s indicated by an arrow in figure 11 and then spread to the next position of a near-wall burst in the spanwise direction (upward in the picture). After the large-scale displacement of fluid, a period ($t^+ = 40$ to 80) of positive skin-friction fluctuation was observed followed by a negative fluctuation.

Based on these flow visualization studies, we can propose a conceptual model for the sequence of burst events (Choi 1985, 1986*a*, *b*) which is shown in figure 14. In stage 1 of the sequence, vortex filaments are deformed by the locally large velocity field created between the pairs of longitudinal vortices which bring the higher-momentum fluid towards the wall. This event is called a near-wall burst. Then the deformed vortex filaments are developed into hairpin loops by self-induction mechanisms in stage 2. After that, the hairpin loops, under the combined velocity field of self-induction and the shear layer, move away from the wall with an angle of about 45° towards the downstream direction (Head & Bandyopadhyay 1981) as shown in stage 3 of the figure. As the hairpin loops move away from the wall during the 'ejection', their neighbouring legs approach each other very closely to form pairs of longitudinal vortices as shown in stage 3. The longitudinal vortices shown on the left (downstream position) of stage 1 are, in fact, formed as the result of this, thus completing a cycle of bursting. Although the image of the counter-rotating pair of

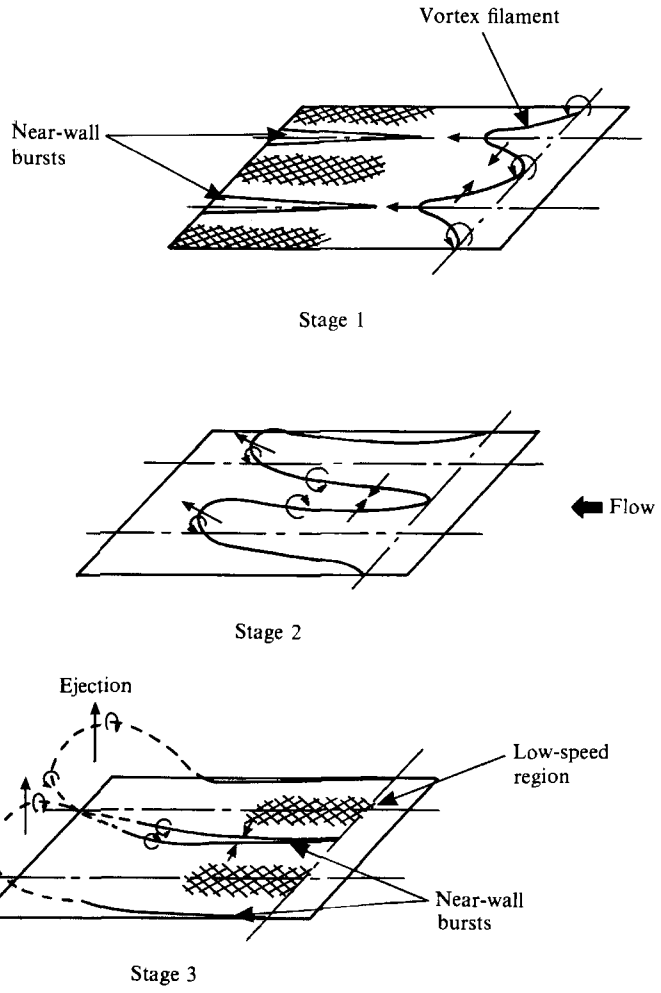

FIGURE 14. Conceptual model for the sequence of burst event. Stage 1, induction of vortex loops; Stage 2, lift-up of hairpin loops; and Stage 3, ejection of hairpin loops and stretching of longitudinal vortices.

longitudinal vortices tends to drive the neighbouring legs apart, the present results of flow visualization indicate that the legs were moved closer together during the ejection phase. This is probably because the stretching of these longitudinal vortices to move the neighbouring legs closer is stronger, overriding the induction by the image vortices.

This conceptual model is similar to the one proposed by Wallace (1982) in that both models are based on a vortex stretching mechanism. The descriptions of near-wall turbulence structure are, however, different especially in the production mechanism of turbulent skin friction during the near-wall bursts. In the present model, the near-wall bursts take place between pairs of counter-rotating longitudinal vortices, where the higher-momentum fluid is induced towards the wall giving rise to a large skin friction. A two-point space correlation measurement conditional on the near-wall burst (Choi 1986*b*) seems to support the present model for the burst sequence.

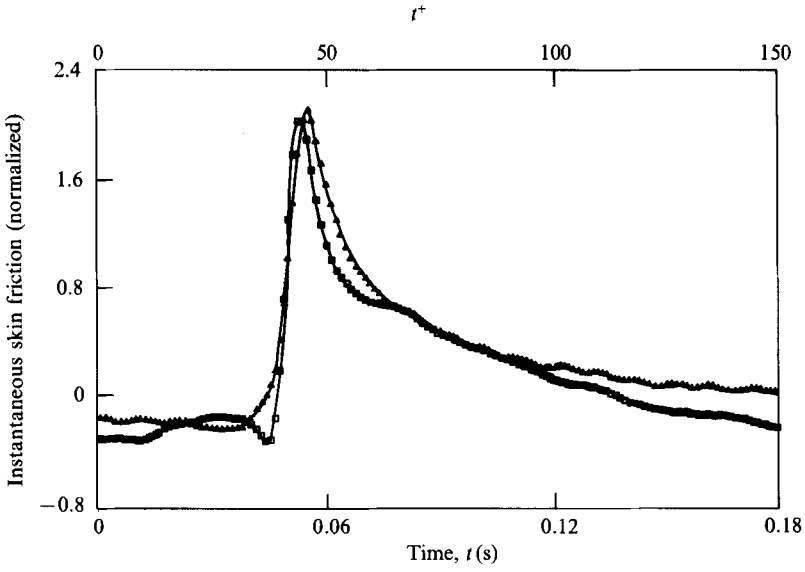

FIGURE 15. Conditionally sampled burst signatures of wall-skin-friction fluctuation over the smooth surface (△) and riblet surface (□), from Choi (1985).

7. Conditional sampling of near-wall turbulence structure

In order to understand the mechanism of drag reduction with riblets, it is important to study the structure of the near-wall bursts as the events are associated with a large increase of skin-friction fluctuation. Here we used the VITA (variable-interval time average) technique to capture the three-dimensional structure of the near-wall bursts. The technique is described in detail by Blackwelder & Kaplan (1976) and Antonia (1981). Basically, in this technique, the running averaged standard deviation of the fluctuating signal from the trigger sensor is examined and used as a reference signal for the conditional sampling. In the present investigation, one of the hot-film sensors mounted flush with the wall surface was taken as the trigger sensor. This detected the instantaneously large increase of skin-friction fluctuation associated with the near-wall bursts. The running average time for the burst detection was set to $t^+ = 12.8$, where t^+ is defined by

$$t^+ = t\frac{u^{*2}}{\nu}. \tag{3}$$

Here t is the averaging time (15 ms with a free-stream velocity of 3 m/s), u^* is the skin-friction velocity, and ν is the kinematic viscosity. For the conditional sampling over the riblet surface, the riblet data were used for setting the threshold value.

Figure 15 shows a comparison of the two signatures during the near-wall burst conditionally sampled over the riblet and smooth surface. It is shown in the figure that the duration of the burst over the riblet surface was about one half of that over the smooth surface. A similar comparison was made by Bacher & Smith (1985). In their work, although the difference in the duration of near-wall bursts is not as clear as in the present study, they found a similar behaviour of burst signature over the riblet surface in which the excursion from negative to positive u-velocity was swifter and had some kind of oscillation or 'wiggle'. Bacher & Smith attributed this wiggle to the 'stabilization' of the low-speed streak by the riblet surface. They argued that

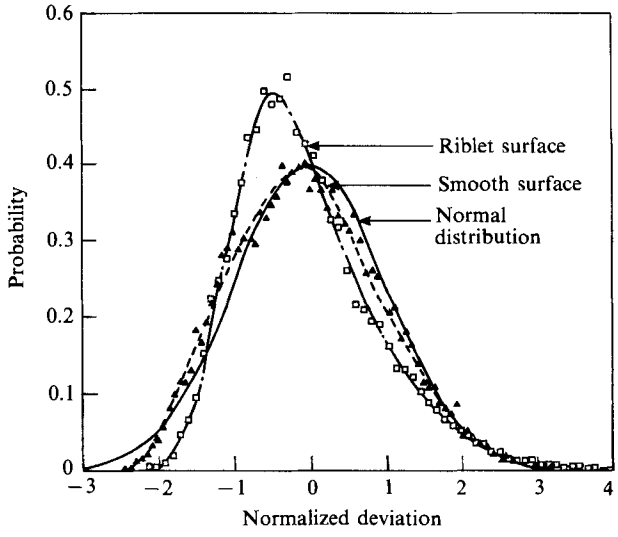

FIGURE 16. Probability density of the wall-skin-friction signal over smooth and riblet surfaces compared to the normal distribution.

the flow sensor would be more prone to detect the regularity of the streak oscillation if the riblet surface reduces the lateral movement of the streaks. It must be noted here that our results shown in figure 15 are the wall-skin friction signal, whilst the results by Bacher & Smith were based on the u-component velocity signal at $y^+ = 14$.

Burst frequency was examined by Choi (1985) for the wall-skin-friction signals over the riblet and smooth surface. It was found that the frequency of the near-wall bursts over the riblet surface was nearly eight times that over the smooth surface. This increase of frequency of the near-wall bursts can be observed in the positive-side tail of probability density shown in figure 16. It also resulted in changes in turbulence statistics. Skewness and kurtosis of the skin-friction signal over the riblet surface was 1.31 and 6.82 respectively compared to 0.42 and 3.12 over the smooth surface.

Hooshmand *et al.* (1983) and Pulles (1988) reported a small but clear increase of burst frequency over the riblet surface. Walsh (1982) and Bacher & Smith (1985), on the other hand, concluded that the burst frequency was essentially unchanged. Gallagher & Thomas (1984) and Savill (1987) showed that the number of bursts were reduced by 20 to 30% with riblets. All of these studies were conducted by using the VITA technique, except for the flow visualization study by Savill. As has been pointed out by Gallagher & Thomas (1984) the number of variables affecting the burst detection is quite large. The digitization rate, integration time, record length, probe size, threshold level and position of probe are some of the affecting variables. In addition, the riblet shape (Pulles 1988) and evaluation method of skin-friction velocity (Hooshmand *et al.* 1983) can also influence the outcome of the burst detection. In the present study, the sensor was mounted flush with the wall surface so that the positioning was different from other studies. Therefore, the results should be interpreted and compared very carefully.

Figure 17 shows an isometric view of the result of the conditional correlation measurement over the smooth surface. The threshold value of 1.00 was used in the conditional sampling. This figure was constructed using fourteen values of two-point

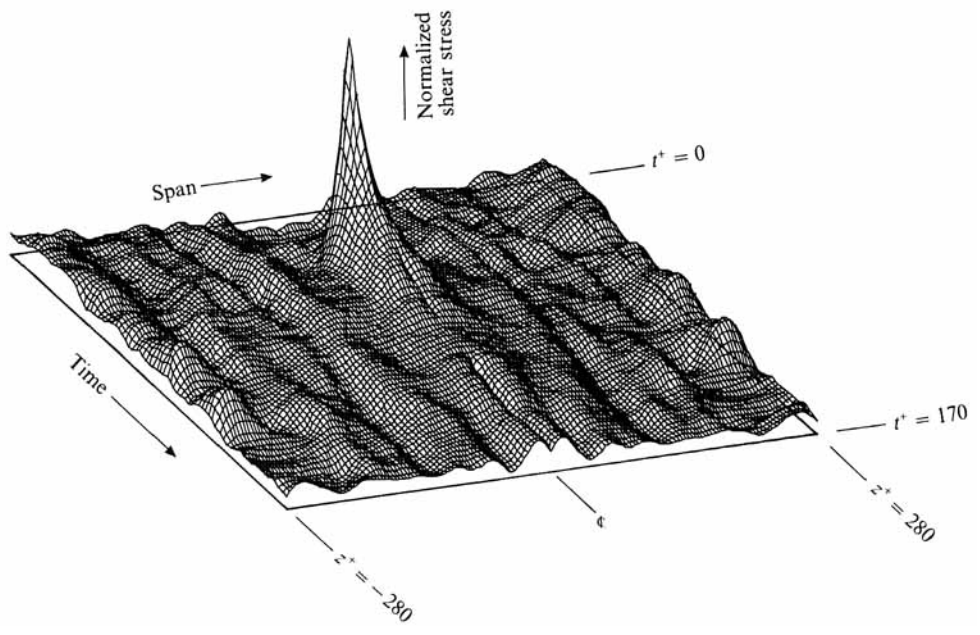

FIGURE 17. Isometric view of the spanwise correlations of wall-skin-friction signal over the smooth surface. The threshold value for the burst detection is 1.00.

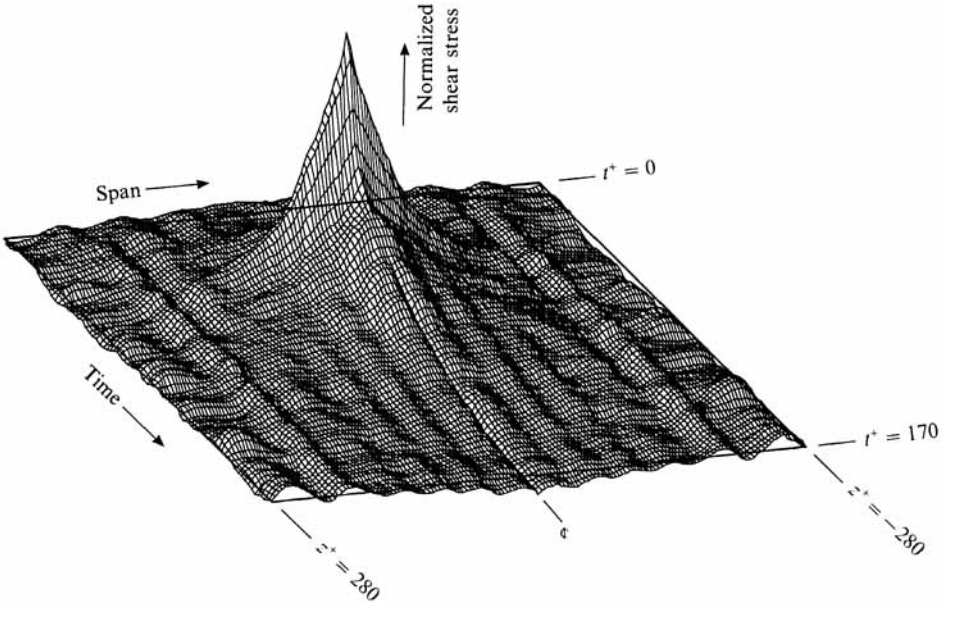

FIGURE 18. Isometric view of the spanwise correlations of wall-skin-friction signal over the riblet surface. The threshold value for the burst detection is 1.00.

conditional correlations from eight non-uniformly spaced sensors, laid out in such a way that the trigger sensor was positioned in the centreline of the figure. Grid points of the figures were obtained by interpolating the fourteen sets of ensemble-averaged time series with cubic splines. The longitudinal ridges seen in the figure indicate the lines of positive correlation of the sampled signal. Therefore the existence of

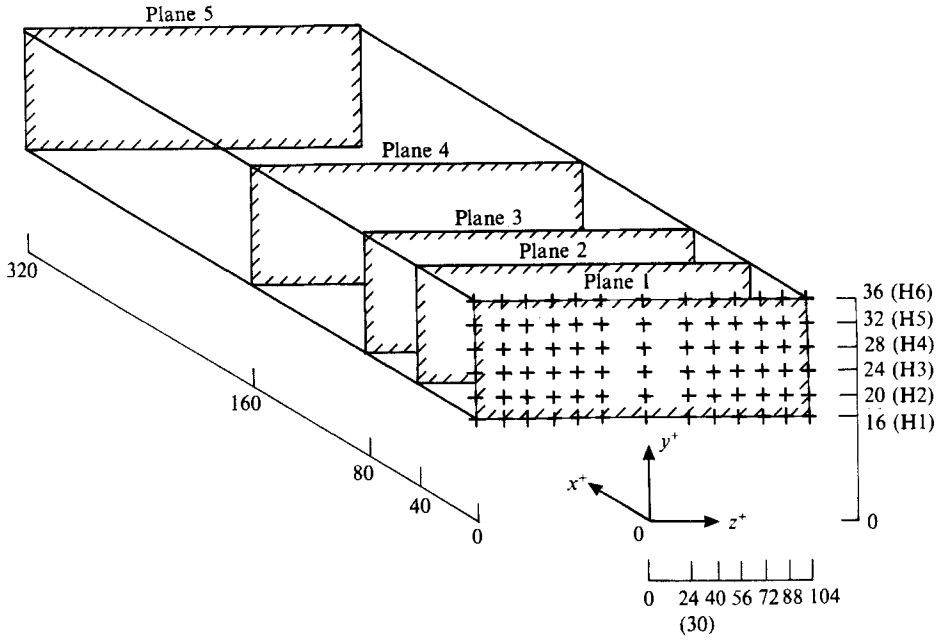

FIGURE 19. Measurement planes and locations for the conditional sampling of the velocity field during the near-wall bursts.

longitudinal ridges in the figure and their spanwise regularity can be interpreted as the near-wall bursts taking place with a regularity in time and space. The mean spacing between the ridges indicates, therefore, the average distance between two near-wall bursts taking place at the same time.

Similar features are shown in figure 18 for measurements over the riblet surface. It is clear from these figures that there is a wider area of positive correlation, about 180 wall units, near the centreline over the riblet surface compared with about 90 wall units for the smooth surface.

It seems that there are several reasons for this wider positive correlation over the riblet surface. The first is due to the spacing between the pair of counter-rotating longitudinal vortices. It was observed by Gallagher & Thomas (1984), Choi (1985) and Bacher & Smith (1985) that the spanwise spacing between the pair over the riblet surface was wider than that over the smooth surface. Choi (1985) argues that this was due to 'premature' bursts as a result of the physical restriction of longitudinal vortices from moving to the spanwise direction by the riblets. The second reason seems to be the position of these vortices relative to the wall sensors. The extent of positive correlation due to the near-wall bursts is wider over the riblet surface as the vortices cannot get closer to the bottom surface due to the presence of riblets. The reduced meandering of longitudinal vortices over the riblet surface observed in the flow visualization may also be a reason for the wider extent of positive correlation.

In order to further investigate the turbulence structure during the near-wall bursts, a study of the velocity field associated with the events was carried out. Two-component velocities were sampled simultaneously from three cross-wires (DISA 55P63) conditional on the occurrence of a large instantaneous increase of wall-skin

friction. Figure 19 indicates the location of the measurements relative to the trigger sensor at the origin. We investigated the velocity field in five planes at $x^+ = 0, 40, 80, 160$ and 320, where data were sampled at thirteen different spanwise locations and six different heights H1 ($y^+ = 16$) to H6 ($y^+ = 36$).

Figures 20 (a, b) and 21 (a, b) show the results of conditionally sampled v- and u-component velocities over a smooth and a riblet surface respectively as a function of time. Only the results at plane 1 ($x^+ = 0$) and plane 5 ($x^+ = 320$) are shown. These figures were constructed in a similar way to figures 17 and 18. There is a clear indication that the near-wall bursts over a smooth surface (figure 20 a, b) were associated with a negative v-component velocity (towards the wall) and positive u-component velocity. This sweep-like behaviour of the near-wall bursts was also found over the riblet surface as shown in figure 21 (a, b). The maximum negative v-component velocity in plane 1 ($x^+ = 0$) was observed at around $t^+ = 40$ when there was the sharpest slope in the burst signature. In the planes further downstream (e.g. figures 20 b and 21 b), the maximum negative v-component velocity was observed at a later time. These results are interpreted to mean that the near-wall bursts were caused by some kind of 'structure' situated above the bursts, which had negative v-component velocity and positive u-component velocity. The time lag observed in plane 5 seems to be due to the time required for the 'structure' to be convected from plane 1 to plane 5. Although it is less clear over the smooth surface, the results over the riblet surface strongly suggest that there was a velocity reversal towards the end of the near-wall burst, where v-component velocity became positive and u-component velocity negative. The spanwise extent of negative v-component velocity near the centreline was about 40 wall units over the smooth surface and 80 wall units over the riblet surface. The v-component velocity was positive outside this region with its maximum value around $z^+ = \pm 40 \sim 60$. The positive u-component velocity was well correlated with the negative v-component velocity.

It seems that the results presented here can be explained if we imagine a flow model such as shown in figure 22. The model has a counter-rotating pair of longitudinal vortices in the measurement volume between plane 1 and plane 5. The sense of rotation is such that the induced velocity is towards the wall. First, the sweep-like behaviour of the near-wall bursts was a result of the induced velocity between the concentrated pair of vortices near the origin. The v-component velocity was therefore, negative between the pair of vortices and positive outside of it. The u-component velocity was positive between the pair because the fluid mass of higher momentum was transported from the above. As the hairpin loops were lifted up during the ejection, the pair of vortices, which are the legs of neighbouring loops, were gradually moved upward, increasing the distance between the pair. Therefore, the extent of negative v-component velocity was widened in the streamwise direction. The reversal of the v- and u-component velocities observed towards the end of the near-wall burst is interpreted as the result of induction by the deformed vortex filament shown in stage 1 of figure 14. Near the end of the near-wall burst, these deformed parts were convected downstream, causing the velocity reversal in both v- and u-component velocities.

From the experimental results we are able to demonstrate that the near-wall bursts, which account for a large part of the production of the turbulent skin friction, are associated with the sweep-like motion. It is also shown that the conditionally sampled velocity profiles are compatible with the conceptual model for the burst sequence (figure 14), suggesting that there exists a pair of longitudinal vortices very

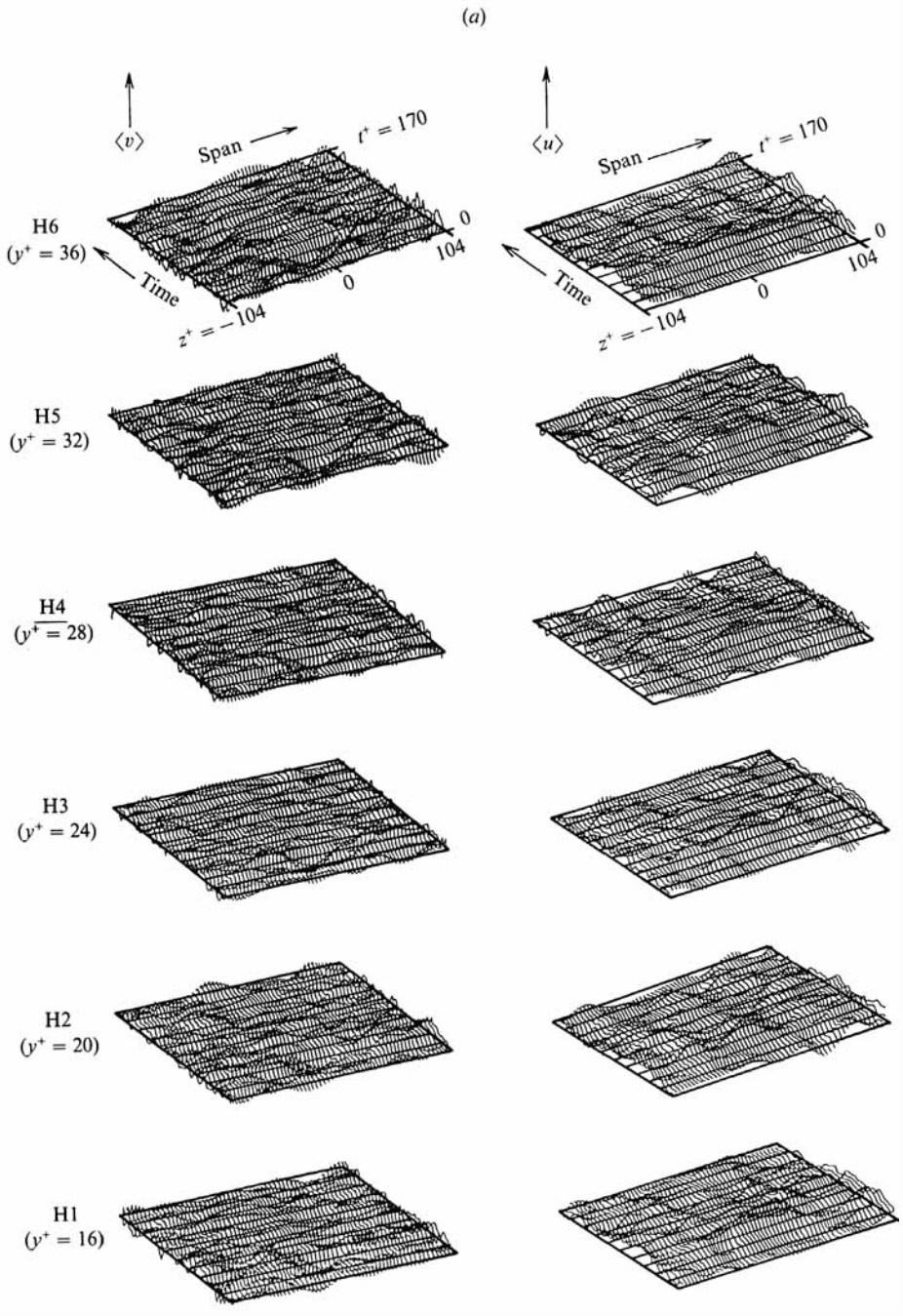

FIGURE 20(*a*). For caption see facing page.

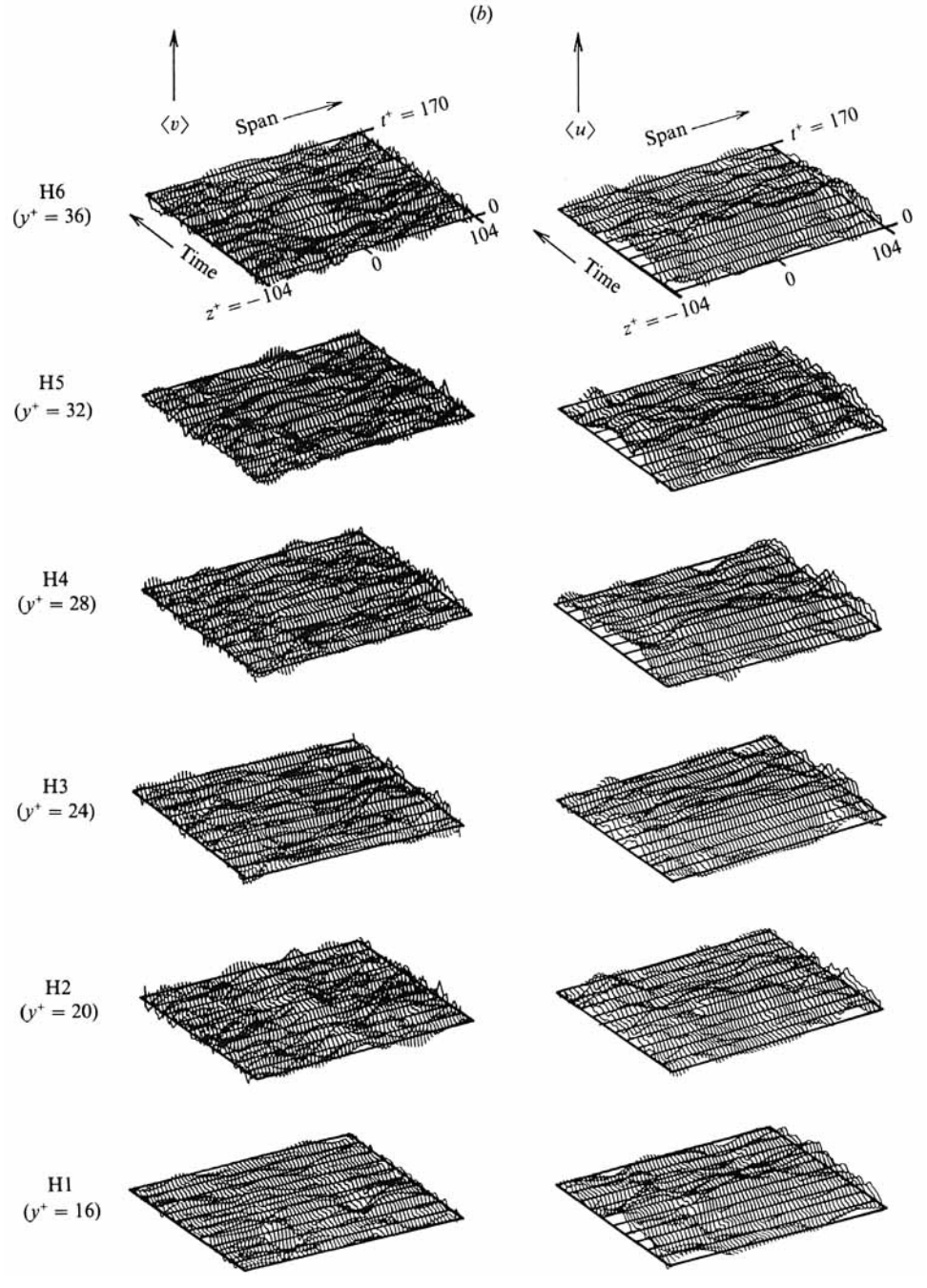

FIGURE 20. An isometric plot of conditionally sampled v- and u-component velocities over the smooth surface at (a) plane 1 and (b) plane 5. H1 to H6 are the distance from the wall surface.

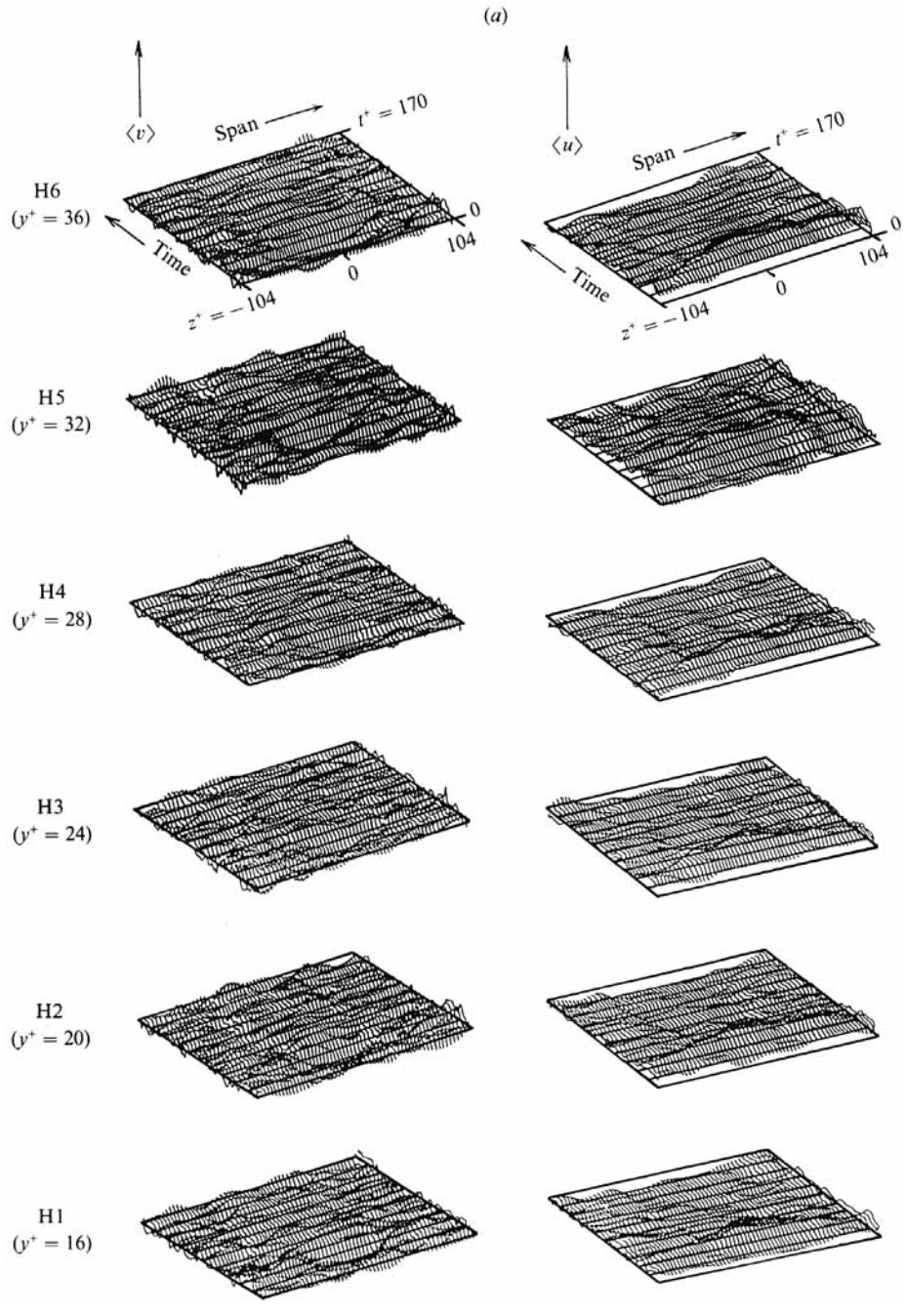

FIGURE 21 (*a*). For caption see facing page.

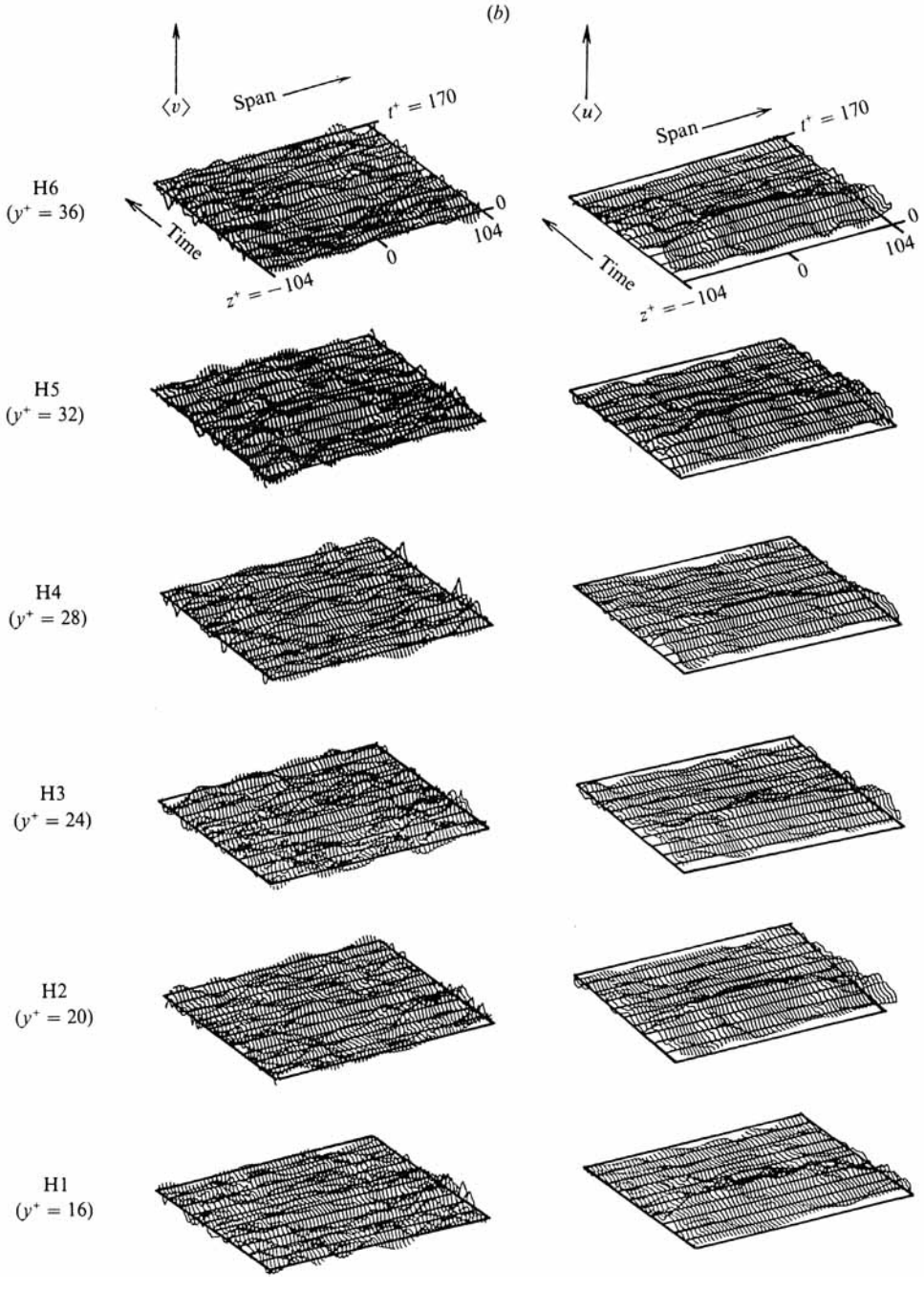

FIGURE 21. An isometric plot of conditionally sampled v- and u-component velocities over the riblet surface at (*a*) plane 1 and (*b*) plane 5. H1 to H6 are the distance from the wall surface.

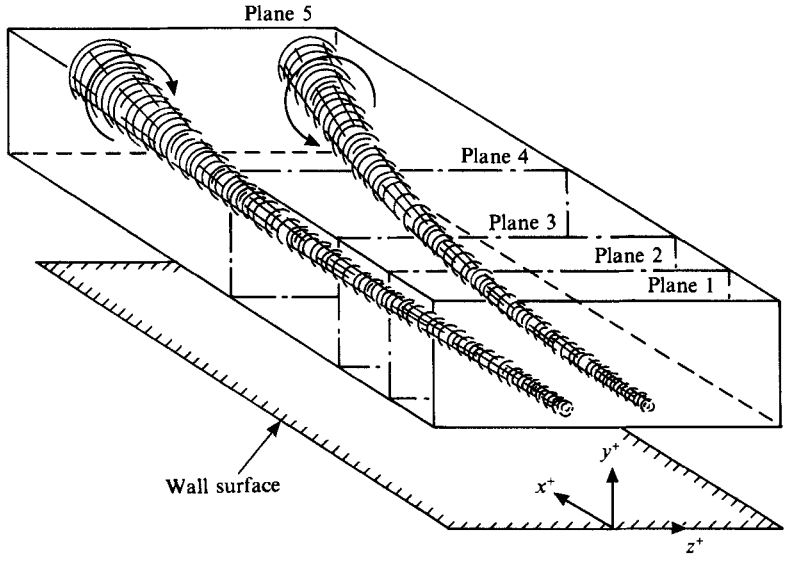

FIGURE 22. A pair of counter-rotating longitudinal vortices constructed from the conditional sampling of the velocity field during the near-wall bursts.

close to the wall surface during the near-wall burst. In order to try and indicate vortex motion associated with the longitudinal vortices, the w-velocity component was computed from the two measured components $\langle u \rangle$ and $\langle v \rangle$ using the continuity equation (Choi 1987*b*). In doing this, an assumption is implicitly made that the change of turbulence structure in the streamwise direction is negligible compared to the change in the other two directions. Owing to this assumption, quantitative accuracy of the results was not expected. Rather, it was hoped to obtain essential features of the turbulence structure during the near-wall bursts. Hatziavramidis & Hanratty (1979) obtained a good agreement with the experimental results by making a similar assumption in the calculation of the turbulent boundary layer close to a smooth wall.

The computed results for $\langle w \rangle$, and the experimental data for $\langle u \rangle$ and $\langle v \rangle$ were used to construct particle paths within the measuring volume (figures 19 and 22), from which the vortex motion associated with the near-wall bursts can be identified. Figures 23 and 24 are respectively plots of the paths of particles released simultaneously from plane 1 for smooth and riblet surfaces. All the particles are viewed from the upstream plane looking downstream. Typically, a particle, which was convected with the mean velocity, stayed about 20 time steps (approximately 20 units in t^+) before it disappeared from the measurement volume at plane 5.

Overall there were similarities in the turbulence structure during the near-wall bursts regardless of the wall surfaces. First, a downwash was observed in the sequences of initial time step, $\Delta t_i = 1$, 20 and 40, followed by an upwash which reversed the flow direction completely ($\Delta t_i = 60$, 80 and 100). Secondly, there seemed to be vortex motion very close to the wall surface at $\Delta t_i = 1$, 20 and 40, below $y^+ = 20$ and around $z^+ = \pm 20$ to 50. This suggests the existence of a pair of counter-rotating vortices responsible for the downwash. The near-wall bursts were detected from the surface sensor at the fortieth time step ($t^+ = 42$) so that the vortex motion

should have been formed before or nearly at the same time as the occurrence of the near-wall bursts. Thirdly there seemed to be another vortex-pair motion for $\Delta t_i = 60$, 80 and 100. The sense of rotation was opposite to the previous vortex motion and the vortices moved closer to the wall after the near-wall burst. The longitudinal vortices identified here, one associated with a downwash during the near-wall burst and the other with an upwash during the ejection, do not conflict. In fact, they are the sequential parts of the near-wall turbulence structure, in which the former located at $y^+ < 20$ is the stretched legs of the latter situated further away from the wall ($20 < y^+ < 35$).

Although the qualitative behaviour of the particle paths over the smooth surface was similar to that over the riblet surface, the quantitative measures were quite different. The spanwise extent of the downwash over the riblet surface was nearly twice as wide as that over the smooth surface, suggesting that the spanwise spacing of the vortex pair over the riblet surface was greater. A similar behaviour is also shown for the upwash during $\Delta t_i = 60$, 80 and 100. Over the smooth surface, a large vortex pair associated with the upwash moved from $y^+ = 28$ at $\Delta t_i = 60$ to $y^+ = 20$ at $\Delta t_i = 100$, with the spanwise spacing of $z^+ = 120$ to 170. Over the riblet surface, on the other hand, the pair started at around $y^+ = 35$ ($\Delta t_i = 60$) and moved to $y^+ = 25$ ($\Delta t_i = 100$). The spanwise spacing was, however, similar to that for the smooth surface.

8. Concluding remarks

A detailed comparative study of the near-wall turbulence structure of the boundary layer over smooth and riblet surfaces has been carried out. The results indicate the following differences in the structure.

First, the mean velocity profile, as well as the turbulence intensity profile, were altered by the surface modification. The mean velocity profile plotted logarithmically was shifted upward, suggesting an increase of viscous-sublayer thickness similar to drag-reducing polymers. The turbulence intensity was reduced by up to 10%. The changes were, however, confined mostly within the wall region. This is in line with the previously published data for a riblet surface. Hooshmand *et al.* (1983) showed from their hot-wire measurements that the spanwise periodicity of the mean velocity almost completely disappears at $y^+ = 13$. Triple correlations obtained by Gallagher & Thomas (1984) were different only in the region $y^+ < 30$. Bacher & Smith (1985) visually observed that the riblets appear to have the greatest effect for $y^+ < 15$. LDA measurement of the higher moments by Pulles (1988) led him to conclude that only the flow in the buffer layer and below is affected by the groove.

Secondly, the fluctuating component of wall skin friction measured with hot-film sensors mounted flush with the bottom surface of the riblets was significantly reduced. The reduction was considered to be a result of a quiescent period for the turbulence observed in the flow. The energy spectrum showed that the reduction was mainly contained in the lower part of the frequency. A similar reduction, although small in magnitude, was found in the spectrum of wall-pressure fluctuation, demonstrating that not only the turbulent skin friction but also the flow noise can be reduced by the manipulation of the turbulent boundary layer with riblets.

Thirdly, the temporal as well as spatial structure of the near-wall burst, believed to be responsible for a large part of the production of turbulent skin friction, were significantly altered by the surface modification. The duration of the near-wall burst

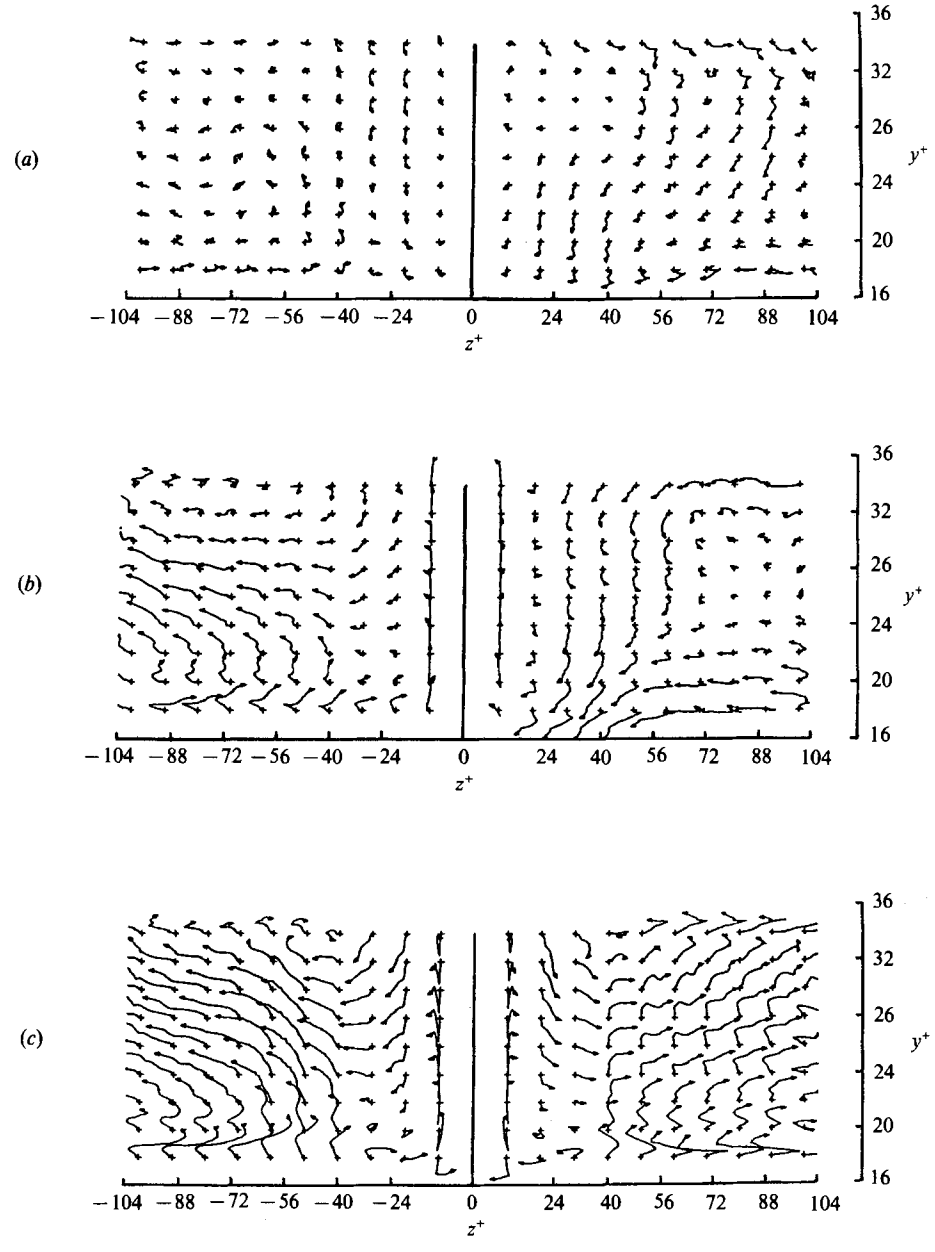

FIGURE 23 (*a–c*). For caption see facing page.

was reduced by a factor of two whereas the burst frequency was substantially increased. The average spanwise spacing between the vortex pairs over the riblet surface was greater than that over the smooth surface.

Fourthly, the near-wall bursts were observed to coincide with the formation of pairs of longitudinal vortices near the wall. These vortices seemed to be the neighbouring legs of hairpin loops as they moved away from the wall during ejection.

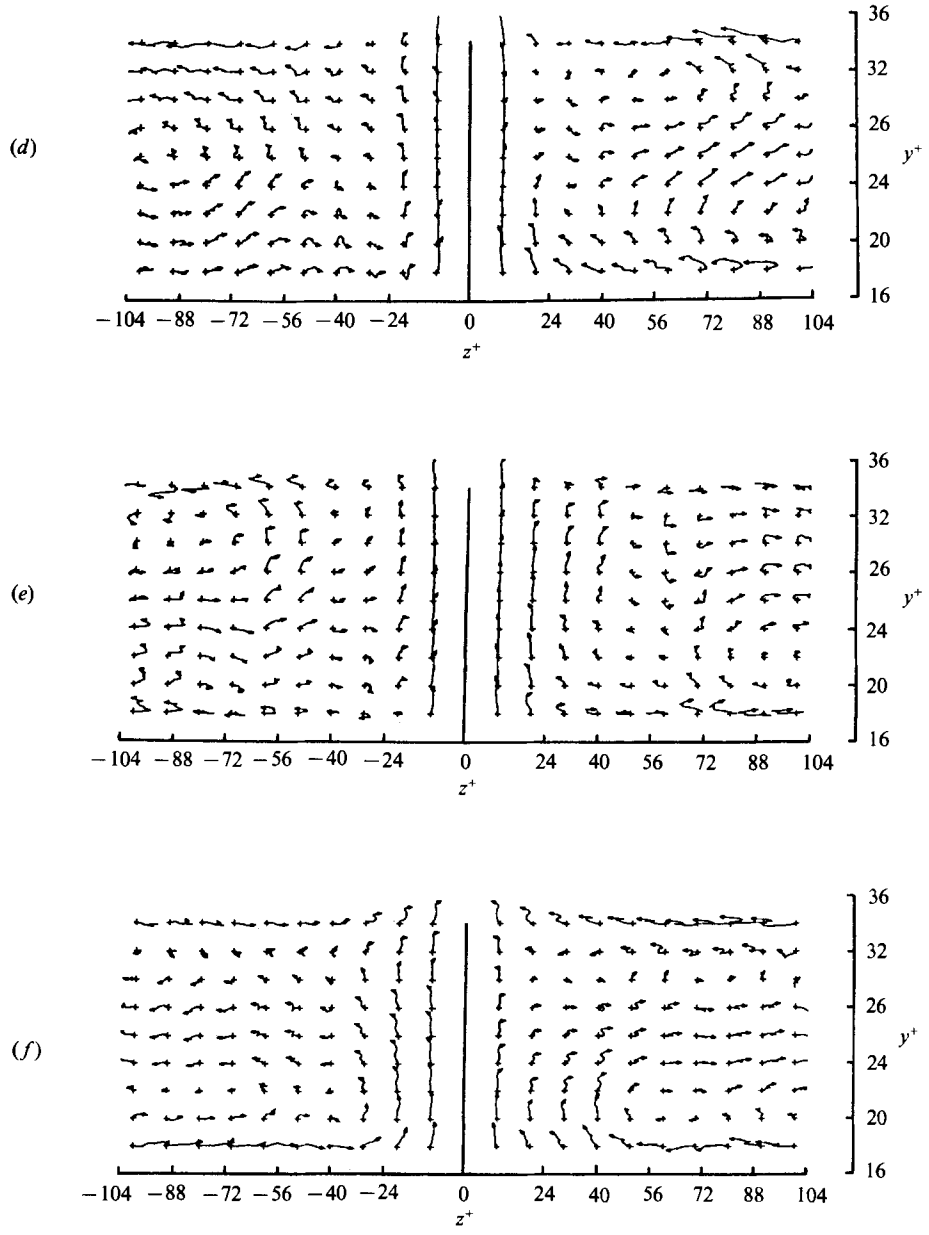

FIGURE 23. Paths of particles in the flow over the smooth surface released from plane 1 at (*a*) initial time step = 1, (*b*) 20, (*c*) 40, (*d*) 60, (*e*) 80 and (*f*) 100.

Flow visualization revealed that pairs of longitudinal vortices over the riblets were less wavy.

Fifthly, the conditionally sampled vertical velocity field of the near-wall bursts indicated that the flow direction during the events was negative, i.e. towards the wall. The negative velocity extended over 80 wall units in the spanwise direction over the riblet surface. There was also a region of positive vertical velocity outside this

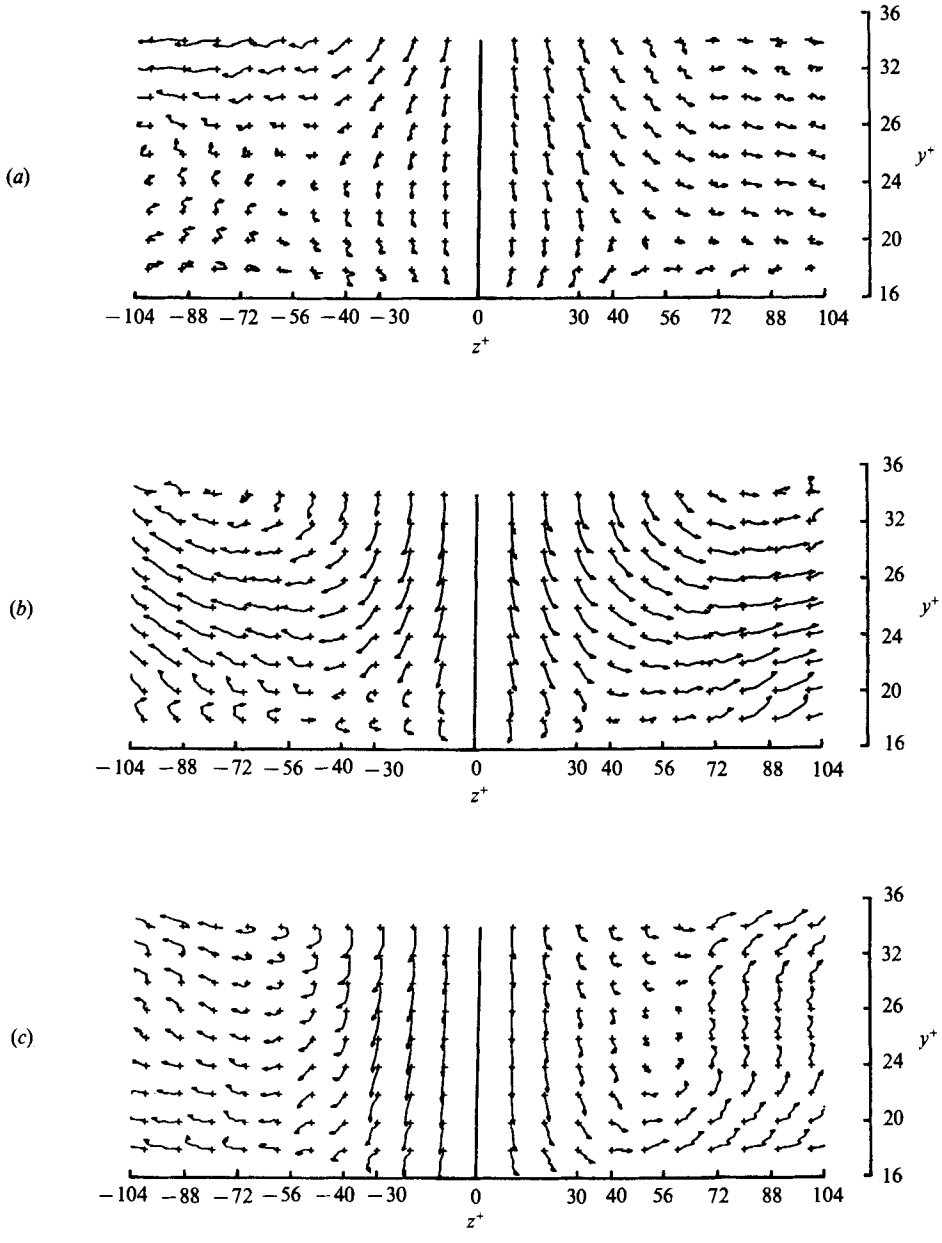

FIGURE 24(a–c). For caption see facing page

negative velocity, which seemed to support the present conceptual model. Similar measurements of the near-wall bursts were obtained over the smooth surface, where the spanwise extent of negative vertical velocity was nearly one half of that over the riblet surface. This is consistent with the results of flow visualization, in which the average spanwise spacing between the pairs of longitudinal vortices over the riblet surface was nearly twice that over the smooth surface.

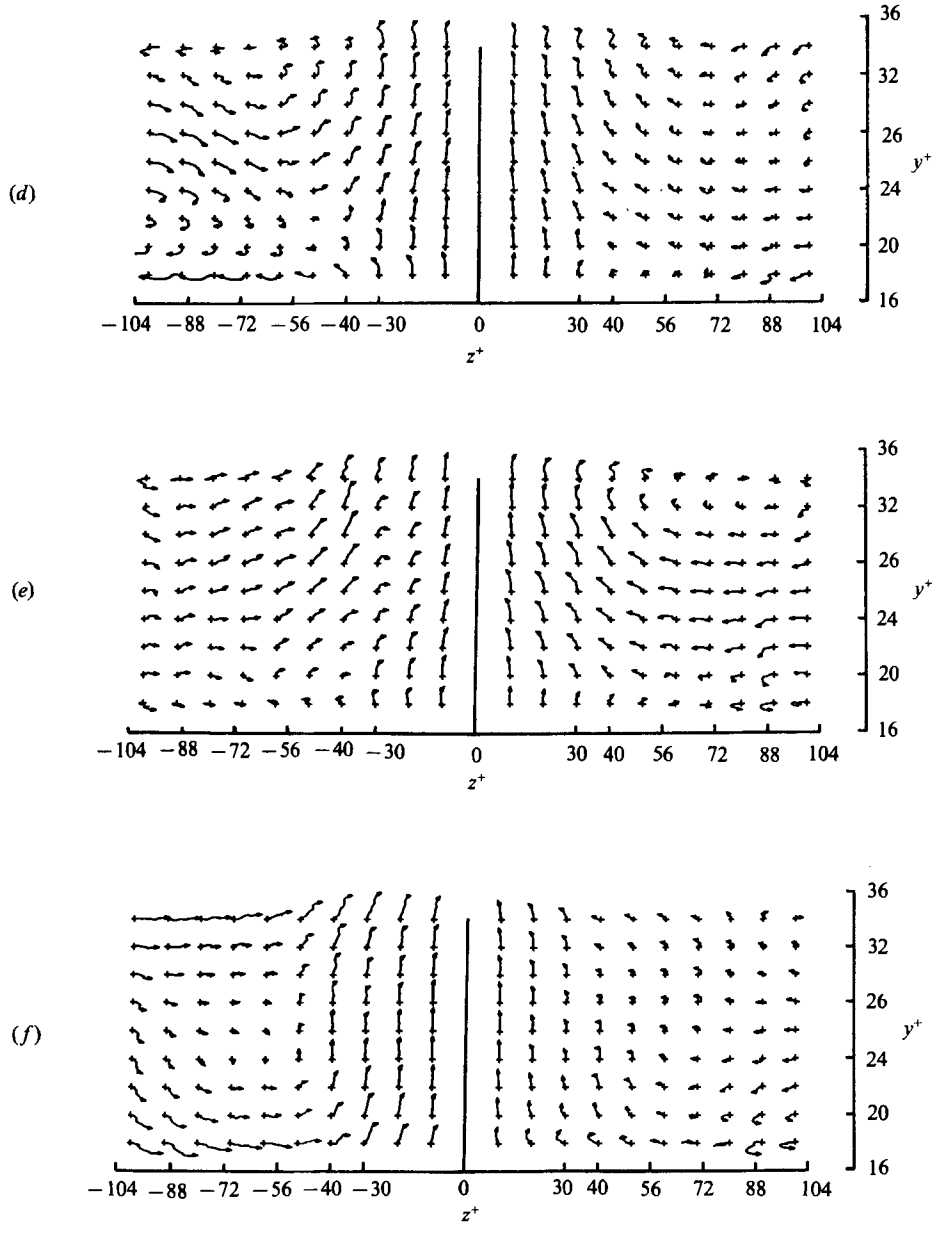

FIGURE 24. Paths of particles in the flow over the riblet surface released from plane 1 at (*a*) initial time step = 1, (*b*) 20, (*c*) 40, (*d*) 60, (*e*) 80 and (*f*) 100.

Lastly, the particle paths during the near-wall burst suggested that there exist two different pairs of longitudinal vortices with opposite rotation, one observed before or during the event and the other after it. The former was located close to the wall ($y^+ < 20$) with a spanwise spacing of between 40 and 100 wall units, while the latter was found further away from the wall ($20 < y^+ < 35$) with a wider spanwise spacing of between 120 and 170 wall units. It is believed that the former is the legs of

neighbouring hairpin loops. The latter seems to be the deformed vortex filaments induced by a large instantaneous velocity field of near-wall burst between the former pair.

As regards possible mechanisms of turbulent drag reduction with riblets, there may be more than one involved. The present study indicates that the restriction of spanwise movement of the longitudinal vortices is a prime mechanism for the turbulent drag reduction. In other words, the spanwise movement of the pair of vortices associated with the near-wall bursts is restricted by the riblets, resulting in a weak premature burst. The turbulent wall skin friction is reduced when this happens as the near-wall burst is one of the main sources for its production. The optimization of riblets should be possible by maximizing the effectiveness of this restriction of the spanwise movement. It is probably not a coincidence that the optimum spacing of the riblets ($10 < s^+ < 25$) is roughly equal to the gap between the longitudinal vortices during the near-wall bursts.

The author would like to express his gratitude to Professor M. Gaster for the support and encouragement during the course of this study. He would also like to extend his acknowledgements to Dr J. A. B. Wills, Dr M. E. Davies and Dr R. Johnson for their valuable discussions. Experimental as well as computational assistance by R. Cooke, Miss K. Croft, Miss M. Aird and B. Collisson is also appreciated. This work has been supported by the Department of Trade and Industry, UK.

REFERENCES

ANTONIA, R. A. 1981 Conditional sampling in turbulence measurement. *Ann. Rev. Fluid Mech.* **13**, 131.

BACHER, E. V. & SMITH, C. R. 1985 A combined visualisation–anemometry study of the turbulent drag reducing mechanisms of triangular micro-groove surface modifications. *AIAA Paper* 85-0548.

BANDYOPADHYAY, P. R. 1986 Review – Mean flow in turbulent boundary layers disturbed to alter skin friction. *Trans. ASME* **I**: *J. Fluids Engng* **108**, 127.

BECHERT, D. W., BARTENWERFER, M., HOPPE, G. & REIF, W.-E. 1986 Drag reduction mechanisms derived from shark skin. *Paper* 86-1.8.3. *15th Congress, International Council of the Aeronautical Sciences, London.*

BECHERT, D. W., HOPPE, G. & REIF, W.-E. 1985 On the drag reduction of the shark skin. *AIAA Paper* 85-0546.

BEELER, G. B. 1986 Turbulent boundary layer wall pressure fluctuations downstream of a tandem LEBU. *AIAA J.* **24**, 689.

BLACKWELDER, R. F. & CHANG, S.-I. 1986 Length scales and correlations in a LEBU modified turbulent boundary layer. *AIAA Paper* 86-0287.

BLACKWELDER, R. F. & KAPLAN, R. E. 1976 On the wall structure of the turbulent boundary layer. *J. Fluid Mech.* **76**, 89.

BROWN, G. L. & ROSHKO, A. 1974 On density effects and large structure in turbulent mixing layers. *J. Fluid Mech.* **64**, 775.

CHOI, K.-S. 1984 A survey of the turbulent drag reduction using passive devices. *NMI Rep.* R-193. NMI Ltd, Feltham, Middlesex, UK.

CHOI, K.-S. 1985 Near-wall turbulence structure on a riblet wall. *BMT Rep.* BMT Ltd, Feltham, Middlesex, UK.

CHOI, K.-S. 1986*a* A new look at the near-wall turbulence structure. in *Advances in Turbulence* (ed. J. Mathieu & G. Comte-Bellot). Springer.

CHOI, K.-S. 1986*b* Drag reduction by manipulation of near-wall turbulence structure. *Proc. European Meeting on Turbulent Drag Reduction, Lausanne* (see also Saville *et al.* 1988).

CHOI, K.-S. 1987*a* The wall pressure fluctuations of modified turbulent boundary layer with riblets. In *Turbulence Management and Relaminarisation* (ed. H. W. Liepman & R. Narasimha). Springer.

CHOI, K.-S. 1987*b* On physical mechanisms of turbulent drag reduction using riblets. In *Transport Phenomena in Turbulent Flows* (ed. M. Hirata & N. Kasagi). Hemisphere.

CHOI, K.-S. & JOHNSON, R. 1989 Effects of pressure gradients on the near-wall turbulence structure with riblets. To be published in BMT Rep. BMT Ltd, Teddington, Middlesex, UK.

CHOI, K.-S., PEARCEY, H. H. & SAVILL, A. M. 1987 Test of drag reducing riblets on a one-third scale racing yacht. *Proc. Int. Conf. on Turbulent Drag Reduction by Passive Means, London.*

COLLIS, D. C. & WILLIAMS, M. J. 1959 Two-dimensional convection from heated wires at low Reynolds numbers. *J. Fluid Mech.* **6**, 357.

COUSTOLS, E. & COUSTEIX, J. 1986 Reduction of turbulent skin friction: turbulence moderators. *Rech. Aerosp.* **1986-2**, p. 63.

COUSTOLS, E. & COUSTEIX, J. 1988 Turbulent boundary layer manipulation in zero pressure gradient. *16th Congress of the Int. Council of the Aeronautical Sciences, Jerusalem.*

DINKELACKER, A., NITSCHKE-KOWSKY, P. & REIF, W.-E. 1987 On the possibility of drag reduction with the help of longitudinal ridges in the walls. In *Turbulence Management and Relaminarisation* (ed. H. W. Liepman & R. Narasimha). Springer.

DJENIDI, L., LIANDRAT, J., ANSELMET, F. & FULACHIER, L. 1988 About the mechanism involved in a turbulent boundary layer over riblets. *Proc. Second European Turbulence Conf., Berlin.*

FURUYA, M. & FUJITA, H. 1966 Turbulent boundary layer over rough gauze surfaces. *Trans. Japan Soc. Mech. Engrs* **32**, 725 (in Japanese).

GALLAGHER, J. A. & THOMAS, A. S. W. 1984 Turbulent boundary layer characteristics over streamwise grooves. *AIAA Paper* 84-2185.

GUEZENNEC, Y. G. & NAGIB, H. M. 1985 Documentation of mechanisms leading to net drag reduction in manipulated turbulent boundary layers. *AIAA Paper* 85-0519.

HATZIAVRAMIDIS, D. T. & HANRATTY, T. J. 1979 The presentation of the viscous wall region by a regular eddy pattern. *J. Fluid Mech.* **95**, 655.

HEAD, M. R. & BANDYOPADHYAY, P. 1981 New aspects of turbulent boundary layer structure. *J. Fluid Mech.* **107**, 297.

HOOSHMAND, D., YOUNGS, R. & WALLACE, J. M. 1983 An experimental study of changes in the structure of a turbulent boundary layer due to surface geometry changes. *AIAA Paper* 83-0230.

JOHANSEN, J. B. & SMITH, C. R. 1983 The effect of cylindrical surface modification on turbulent boundary layers. *Rep.* FM-3. Dept. of Mechanical Engineering and Mechanics, Lehigh University, Pennsylvania.

JOHANSSON, A. V. & ALFREDSSON, P. H. 1985 Recent developments of drag reduction methods for ships. *Proc. Second Int. Symp. on Ship Viscous Resistance, Sweden.*

KLEBANOFF, P. S. 1955 Characteristics of turbulence in a boundary layer with zero pressure gradient. *NACA Rep.* 1247.

KLINE, S. J., REYNOLDS, W. C., SCHRAUB, F. A. & RUNSTADLER, P. W. 1967 The structure of turbulent boundary layers. *J. Fluid Mech.* **30**, 741.

LUMLEY, J. L. 1973 Drag reduction in turbulent flow by polymer additives. *J. Polymer Sci.* D: *Macromol. Rev.* **7**, 263.

MCLEAN, J. D., GEORGE-FALVY, D. N. & SULLIVAN, P. P. 1987 Flight-test of turbulent skin-friction reduction by riblets. *Proc. Intl Conf. Turbulent Drag Reduction by Passive Means, London.*

NGUYEN, V. D., SAVILL, A. M. & WESTPHAL, R. V. 1987 Skin friction measurements following manipulation of a turbulent boundary layer. *AIAA J.* **25**, 498.

NIEUWSTADT, F. T. M., VAN DAM, W., LEIJDENS, H. & PULLES, C. 1986 Some turbulence measurements above a grooved wall. *Proc. European Drag Reduction Conf., Lausanne* (see also Savill *et al.* 1988).

PATEL, V. C. 1965 Calibration of the Preston tube and limitations of its use in pressure gradients. *J. Fluid Mech.* **23**, 185.

PULLES, C. J. A. 1988 Drag reduction of turbulent boundary layers by means of grooved surfaces. Ph.D. thesis, Technical University of Eindhoven.

REIDY, L. W. 1987 Flat plate drag reduction in a water tunnel using riblets. *Naval Ocean Systems Center TR*1169.

REIDY, L. W. & ANDERSON, G. W. 1988 Drag reduction for external and internal boundary layers using riblets and polymers. *AIAA Paper* 88-0138.

SANDBORN, V. A. 1981 Control of surface shear stress fluctuations in turbulent boundary layers. *Rep.* CER 80-81-VAS46. Dept. of Civil Engng, Colorado State University.

SAVILL, A. M. 1987 Effect on turbulent boundary layer structure of longitudinal riblets alone and in combination with outer devices. In *Flow Visualisation IV* (ed. L. Charnay). Hemisphere.

SAVILL, A. M., TRUONG, T. V. & RYHMING, I. L. 1988 Turbulent drag reduction by passive means: a review and report on the first European drag reduction meeting. *J. Méc. Theor. Appl.* **7**, 353.

SAWYER, W. G. & WINTER, K. G. 1986 The effect of turbulent skin friction of surfaces with streamwise grooves. *Proc. European Meeting on Turbulent Drag Reduction, Lausanne* (see also Savill *et al.* 1988).

SMITH, C. R. & METZLER, S. P. 1983 The characteristics of low-speed streaks in the near-wall region of a turbulent boundary layer. *J. Fluid Mech.* **129**, 27.

SQUIRE, L. C. & SAVILL, A. M. 1987 Some experiences of riblets at transonic speeds. *Proc. Intl Conf. Turbulent Drag Reduction by Passive Means, London.*

VIRK, P. S. 1975 Drag reduction fundamentals. *AIChE J.* **21**, 625.

WALLACE, J. M. 1982 On the structure of bounded turbulent shear flow: a personal view. In *Developments in Theoretical and Applied Mechanics, XI* (ed. T. J. Chung & G. R. Karr). University of Alabama, Huntsville, Alabama.

WALSH, M. J. 1980 Drag characteristics of V-groove and transverse curvature riblets. In *Viscous Drag Reduction* (ed. G. R. Hough). American Institute of Aeronautics and Astronautics.

WALSH, M. J. 1982 Turbulent boundary layer drag reduction using riblets. *AIAA Paper* 82-0169.

WALSH, M. J. & LINDEMAN, A. M. 1984 Optimisation and application of riblets for turbulent drag reduction. *AIAA Paper* 84-0347.

WALSH, M. J. & WEINSTEIN, L. M. 1978 Drag and heat transfer with small longitudinal fins. *AIAA Paper* 78-1161.

WILKINSON, S. P., ANDERS, J. B., LAZOS, B. S. & BUSHNELL, D. M. 1987 Turbulent drag reduction research at NASA Langley – progress and plans. *Proc. Intl Conf. on Turbulent Drag Reduction by Passive Means, London.*